Renewable Energy 217 (2023) 119112

Contents lists available at ScienceDirect

Renewable Energy

journal homepage: www.elsevier.com/locate/renene

Hybridization solutions for solar dish systems installed in the Mediterranean region

Giuseppina Ciulla [a,*], Stefania Guarino [a], Michela Lanchi [b], Marco D'Auria [b], Maurizio De Lucia [c], Michele Salvestroni [c], Vincenzo Di Dio [a]

[a] University of Palermo, Engineering Department, Italy

[b] ENEA (Italian National Agency for New Technology, Energy and Sustainable Economic Development), Casaccia Research Centre, Rome, Italy

[c] University of Florence, Department of Industrial Engineering, Italy

ARTICLE INFO

Keywords:
Solar dish concentrator
Direct normal irradiance
Concentrating solar power
Hybridization
Parametric analysis

ABSTRACT

One of the main challenges facing the commercialization of parabolic solar systems is their high initial cost, which is not competitive with the low cost, ease of operation, and reliability of photovoltaic technology. However, one potential solution to maximize their energy producibility and improve their economic profitability is to hybridize the power conversion unit. By enabling reliable power generation and reducing reliance on the availability of solar thermal energy, hybridization can be a valid solution to improve the efficiency and practicality of parabolic dish solar systems. This study aims to assess the energy performance of two hybrid parabolic dish systems: the dish-Stirling system located at the University of Palermo, and the dish-Micro Gas Turbine system located at ENEA Casaccia. Different scenarios were examined by varying the installation site and operational strategy, as well as exploring hybridization solutions of the solar source with conventional fossil fuel or renewable ones. The findings suggest that hybridizing parabolic dish systems with conventional fuels or renewable energies greatly enhances their performance, increasing operational hours and maximizing energy producibility.

1. Introduction

Solar energy is the most effective and sustainable source of clean energy and is considered the main strategic energy source for the energy sustainability of the planet [1–3]. In the world, the area with the greatest potential for solar energy is the "Sun Belt", which is located between 35° north and south of the equator and includes the Middle East, North Africa, South Africa, India, the southwest of the United States, Mexico, Peru, Chile, Western China, Australia, southern Europe, and Turkey. Concentrating solar power (CSP) technologies are a promising alternative to fossil-based technologies to achieve national and global targets for green [4,5], safe and low-cost [6,7] renewable energy generation. CSP technologies use reflectors to collect the beam solar radiation and concentrate it on the surface of a receiver system. The energy concentrated on the receiver guarantees the achievement of high-temperature levels; furthermore, the small aperture area ensures low heat losses by radiation and convection. In general, CSP technologies are mainly classified into point and line focusing technologies [8,9]: solar towers and parabolic dish systems belong to the first group, while linear Fresnel reflectors and parabolic trough collectors belong to the second group [10,11].

Among them, the parabolic dish technology uses a paraboloidal reflector that can be coupled to two types of power conversion units: Stirling engine and gas turbine. In a dish-Stirling system, a Stirling engine is coupled to the focal point of the parabolic dish. The concentrated sunlight heats the Stirling engine's working fluid, usually a gas, causing it to expand and drive a piston or a rotary mechanism. This mechanical motion is then converted into electricity by a generator. The Stirling engine operates based on the temperature difference between the hot and cold sides, utilizing the high-temperature solar energy focused by the parabolic dish [12–14]. In the dish gas turbine system, concentrated solar energy is used to generate high-temperature thermal energy, which is then utilized to drive the gas turbine. The turbine's rotation generates mechanical energy that is converted into electricity through a generator. The gas turbine typically operates based on the expansion of hot gases, and the concentrated solar energy provides the necessary heat input [13,

* Corresponding author.
E-mail addresses: giuseppina.ciulla@unipa.it (G. Ciulla), stefania.guarino@deim.unipa.it (S. Guarino), michela.lanchi@enea.it (M. Lanchi), marco.dauria@enea.it (M. D'Auria), delucia@unifi.it (M. De Lucia), michele.salvestroni@unifi.it (M. Salvestroni), vincenzo.didio@unipa.it (V. Di Dio).

https://doi.org/10.1016/j.renene.2023.119112
Received 30 March 2023; Received in revised form 6 July 2023; Accepted 3 August 2023
Available online 3 August 2023

15,16].

Both systems offer advantages and considerations. Stirling engines are known for their high efficiency, reliability, and ability to operate at lower temperature differentials. On the other hand, gas turbines offer higher power output and faster response times, making them suitable for grid integration and meeting fluctuating electricity demands.

Both are characterized by high operating temperatures and concentration ratio values. Furthermore, these collectors occupy a smaller surface area for the same installed peak power than other types of CSP systems. The typical capacity of these systems varies between 3 and 30 kWp, making them suitable for distributed generation, and providing electricity to rural areas that may be isolated from the grid [17]. However, the high initial cost of parabolic dish concentrators represents a significant challenge for commercializing renewable electricity generation technologies, as they must compete against the low cost, ease of operation, and reliability of photovoltaic (PV) technology [18]. On the other hand, parabolic dish concentrators, differently from PV systems, are intrinsically suitable for on-demand heat and electricity generation.

Various companies worldwide have commercially developed parabolic dish concentrators, and several studies and projects have focused on them. For instance, a 50 MW demonstration plant was constructed in Jodhpur, India, with unit power of 25 kW. For this plant, it was indicated that the annual energy and exergetic efficiencies were improved by approximately 11.52% and 12.35%, respectively [19]. In Almeria, Spain, the authors of [20] conducted an experimental analysis of a parabolic dish system that generated 10.85 kW of electrical power and had a total efficiency of 22.5%. In Hunan, China, the authors of [21] designed and examined a CSP plant that uses a parabolic disc concentrator with an aperture diameter of 17.7 m, a cavity receiver with an outside diameter of 0.275 m, and an α-type Stirling engine. This plant achieved a net electric peak power of 38.8 kW with an overall efficiency of 25.3%. The parabolic dish system built by Stirling Energy Systems (SES) in California (USA) [13] instead achieved a peak conversion efficiency of about 28% and an electric output power of 24.9 kW. In Arizona, USA, a 1.5 MW plant was recently constructed and connected to the grid; it has 60 dish concentrators with reflectors featuring a silver-plated glass upper surface. The maximum nominal efficiency of the plant was estimated to be 29.6% [22].

Mathematical modeling plays a key role in the development of parabolic dish technology, enabling the optimization of control techniques and the accurate estimation of electrical producibility, thus promoting the widespread adoption of parabolic dish solar concentrators. In the literature, several studies and attempts can be found that aim to simulate a CSP system accurately. In 1985, it was found that the performance of the concentrator was influenced by the effect of the tracking system's optical errors, and the rim angle of the concentrator influenced the receiver's temperature [23]. In 2005, the authors of [24] conducted a theoretical investigation to maximize the power and efficiency of a dish-Stirling system by determining the optimal receiver temperature. The results obtained showed that an increase in concentrated solar intensity led to an increase in both the optimum absorber temperature and the maximum overall efficiency, whereas a decrease in engine cooling temperature resulted in a decrease in the optimum temperature of the absorber and an increase in the maximum overall efficiency. In Ref. [25], the authors presented a mathematical model to control and optimize a CSP system, which correlated solar energy with the mechanical, thermal and electrical energies generated by the system, considering the thermodynamic cycle, heat transfer processes in the receiver and concentrator, mechanical dynamics, and the heat flux in the Stirling engine. In contrast, in Ref. [26], the authors developed a thermodynamic optimization model for a Stirling engine based on the finite heat transfer rate and regenerative heat losses of the engine. The model maximized the power and efficiency of the engine and minimized the generation of entropy. In Ref. [27], some authors investigated how the geometric parameters of the paraboloidal reflector could influence the performance of a parabolic dish system. For example, they developed a MATLAB code to model and simulate a parabolic dish solar concentrator, considering the effect of many operating factors typical of the dish reflector, such as the material, geometry, aperture area of both the parabola and receiver, focal length and focal point position, concentration ratio, and rim angle, etc [28]. A multi-objective optimization study was conducted in Ref. [29], where a genetic algorithm integrated with a mathematical simulation developed in FRONTIER was used to optimize the design of a dish-Stirling system.

The integration of a parabolic dish CSP system with thermal energy storage or the combination with alternative energy sources is becoming increasingly prominent. Hybridization is a promising avenue to enhance the efficiency and practicality of dish-Stirling systems, mainly by enabling reliable power generation and reducing dependence on the availability of solar thermal energy [30].

Numerous studies have explored the concept of combining dish-Stirling systems with alternative energy sources. Monné et al. conducted a comprehensive energy analysis and life cycle assessment of two possible configurations for a 10 kWe hybrid dish-Stirling system, comparing the use of natural gas and biogas in Seville, Spain. Results showed that hybridization can be beneficial depending on the type of fuel utilized, with biogas proving to be the most effective option [31,32]. Meanwhile, Hartenstine et al. utilized numerical simulations and small-scale tests to evaluate the feasibility of a hybrid receiver that was designed to achieve a minimum overall thermal efficiency of 80%. Their work aimed to demonstrate that a heat pipe receiver can operate using multiple energy sources simultaneously, and the successful fabrication of a full-scale hybrid receiver showcased the potential for maximum and continuous electrical output [33]. Other researchers, such as Blázquez et al., Barbosa et al., Kang et al., Laing et al., and Moreno et al., have also explored the optimization, testing, and development of hybrid dish-Stirling systems, focusing on areas such as concentrator geometry, receiver cavity requirements, heat transfer characteristics, and combustion systems [34–38]. In Ref. [39], it is demonstrated that hybridization could ensure good power source stability and meets the autonomy requirements of the system.

In this framework, this study delves into the hybridization of the energy input resource of a parabolic dish solar concentrator by analyzing the energy performance of two existing systems: a dish-Stirling concentrator installed at the University of Palermo (UNIPA) campus in southern Italy and a dish Micro Gas Turbine (MGT) concentrator installed at the ENEA Casaccia research center near Rome in central Italy. It is important to emphasize how the reference to existing solar concentrators, whose energy modeling is based on real operational data, allowed for an accurate and realistic evaluation of the performance of hybrid systems. Moreover, various operational strategies were examined, taking into account possible solutions for the hybridization of the solar source with conventional or renewable fossil fuels. Additionally, a parametric analysis was carried out to evaluate and compare these two systems in different climatic contexts, considering five locations in the Mediterranean area with varying levels of solar beam irradiation: Casaccia (Italy), Marrakech (Morocco), Palermo (Italy), Tabuk (Saudi Arabia), and Ragusa (Italy). For each hybridization scenario and each location studied, several key parameters were identified, such as cycle efficiency, solar share, capacity factor and avoided greenhouse gas emissions, to assess the impact of hybridization and latitude of the site in a system of solar dishes.

To provide a clear overview, this paper is structured into the following sections: Section 2 presents the adopted approach and methodology for analyzing the producibility of the examined parabolic dish systems, operating both in solar and hybrid modes. In Section 3, the dish-Stirling system installed at the University of Palermo is described, along with the energy model used to estimate its producibility, including hybrid operation. Section 4 covers the dish-MGT system installed at the ENEA research center, presenting the energy model and the hybrid alternative of the system. Moving on to Section 5, the results of the climate data analysis for the various examined installation locations and the annual simulations conducted for the two investigated parabolic dish systems are presented. Finally, Section 6 summarizes the most significant conclusions drawn from the entire study.

2. Approach and method

An effective solution to maximize the energy production of solar parabolic concentrators and improve their economic profitability is to hybridize the power conversion unit, thereby mitigating the issue of the variability of solar energy. This approach has the potential to make a parabolic dish solar concentrator highly competitive in terms of dispatchability and adaptable to the local energy context by utilizing available renewable or non-renewable resources. Specifically, the external combustion engine of the Stirling engine can be hybridized. A hybrid dish-Stirling solar concentrator could operate for extended periods, even during times when solar radiation is not available [32]. The Stirling engine in a hybrid dish-Stirling system could be powered by thermal energy generated from the combustion of natural gas, syngas, or biogas. Similarly, to stabilize the electrical output and/or extend the production of electricity of a dish-MGT system, conventional hybridization solutions can be applied by integrating combustors commonly used in the energy or automotive sector with gas turbines. Also, in this case, the solar source could be supported by fuel gases to obtain a rapid response to changes in the system load (natural gas, syngas or biogas), and the combustor could be integrated into the circuit in different configurations, as described in detail in the following sections.

In this study, reference was made to two parabolic dish solar concentrators installed in Italy.

- the dish-Stirling demonstration plant system at UNIPA, installed in 2017 and produced by Swedish company Ripasso Energy [40]. This system combines a paraboloidal reflector with a Stirling engine and has a net electric peak output power of 31.5 kW (under direct normal irradiance of 960 W/m^2, ambient temperature of 25 °C, and clean mirrors). It also holds the record for the highest solar-to-electric conversion efficiency of 32% (achieved at the Upington, South Africa test site) [22];
- The dish-MGT demonstration prototype at the research center of ENEA Casaccia, recently developed by ENEA in collaboration with a European consortium [15], features a unique element where the Stirling engine is replaced with a Micro Gas Turbine, a technology commonly used in the automotive industry, in order to achieve a more reliable and cost-effective plant. The use of MGT, which features compact and lightweight motors with no periodic movements, operating at low pressures (<5 bar), aims to reduce the frequency and cost of maintenance operations, especially in remote geographic contexts where skilled labour may not be readily available.

Three different combustible gases were considered for the hybridization of the power conversion units of the reference solar concentrators: natural gas, syngas, and biogas. The Low Heating Values (LHV) of these gases are listed in Table 1.

Natural gas is mainly composed of methane (CH_4) and has the lowest environmental impact compared to other commonly used fuels. Its carbon dioxide (CO_2) emissions are 40–50% and 25–30% lower than those of coal and fuel oil, respectively. Determining the CO_2 emissions of natural gas is very simple since its composition is almost the same regardless of its specific origin [41]. An LHV equal to 35 MJ/Nm^3 and a CO_2 emissions conversion factor equal to 1.86 kg CO_2/m^3 were assumed [42]. Syngas, produced through gasification, has gained significant attention in recent years as a renewable energy source since the carbon dioxide released by its use is balanced by the sequestration of carbon dioxide by plants during photosynthesis. Biomass syngas typically has an LHV that is equal to 5 MJ/Nm^3 [43]. Biogas, on the other hand, is usually characterized by 50–75% methane, with the rest primarily being CO_2 [41]. In the methane combustion process, CO_2 is also produced, but these emissions are considered to have a zero net balance, as they are framed in the carbon cycle. The reason is that the CO_2 emitted in both gas production and methane combustion is the same that would naturally be produced by the biological degradation of waste. Thus, biogas is usually considered renewable energy with zero CO_2 emissions. The properties of syngas depend on several factors including the type of primary energy resource used, the type of gasifier, the oxidizing agent used and the temperature and pressure conditions that characterize its operation [44]. An LHV of 23 MJ/Nm^3 is assumed for biogas [41]. Unlike natural gas, the use of biogas or syngas is linked to the availability of generation plants in the surrounding area where the dish-Stirling system is installed [41].

To evaluate and compare the performance of the UNIPA-Stirling and the ENEA-MGT solar concentrators, a comprehensive parametric analysis was carried out, taking into account various hybridization strategies and five different locations in the Mediterranean region, since the performance of both solar systems is significantly affected by the direct normal irradiation. Table 2 presents the annual DNI values for each of the five locations that include and include Casaccia, the current installation site in central Italy for the dish-MGT system developed by ENEA; Marrakesh, one of the largest cities in Morocco located in the center south of the country; Palermo, that is located in the southern part of Italy and the actual installation site for the dish-Stirling of UNIPA; Tabuk, a city of Saudi Arabia; and Ragusa, a city in the south-eastern part of Italy.

To assess the energy performance and environmental benefits of the two analyzed concentrated solar systems, considering different locations and hypothesized hybridization scenarios, and to enable a fair comparison between the two systems, the following quantities were calculated.

a. Annual electricity production (E_t) of the solar concentrator, defined as the amount of net electricity generated by the system in a year

$$E_t = \sum_{i=1}^{i=8760} E_i \left[\frac{MWh}{year}\right] \quad (1)$$

where E_i is the net electricity produced in the i-th progressive hour of the year.

b. Conversion efficiency of solar energy into electricity ($\eta_{sol-ele}$) or overall efficiency of the solar concentrator, defined as the ratio between the net electricity produced (E_i) and the solar energy collected by the reflector on an annual basis:

$$\eta_{sol-ele} = \frac{E_t}{\sum_{i=1}^{i=8760} (DNI_i \cdot A_n)} \cdot 100\ [\%] \quad (2)$$

Table 1
LHV of natural gas, syngas, and biogas.

Fuel	LHV [MJ/Nm^3]
Natural gas	35
Syngas	5
Biogas	23

Table 2
Selected locations and annual DNI values (solar database: Meteonorm) [45].

Locations	DNI[a] [kWh/m^2/year]
Casaccia (Italy)	1724.3
Marrakesh (Morocco)	2454.2
Palermo (Italy)	1932.6
Tabuk (Saudi Arabia)	2876.3
Ragusa (Italy)	2138.3

[a] Meteonorm database (period: 1991–2010).

where DNI_i is the hourly direct solar irradiance typical of the selected location and A_n is the net area of the reflector [46].

c. Thermodynamic efficiency of the cycle (η_M), defined as the ratio between the mechanical energy produced by the engine (eg. Stirling, MGT) (W_S) and the high-temperature thermal input energy of the same engine (Q_S) [47], calculated on an annual basis:

$$\eta_M = \frac{W_S}{Q_S} \cdot 100\ [\%] \tag{3}$$

d. Thermal efficiency of the engine (η_T), defined as the ratio between the thermal energy produced by the engine (eg Stirling) at low temperature ($Q_S - W_S$) and the high-temperature thermal input energy of the same engine (Q_S) [47], calculated on an annual basis:

$$\eta_T = \frac{(Q_S - W_S)}{Q_S} \cdot 100\ [\%] \tag{4}$$

e. Primary Energy Ratio (PER), defined as the ratio between the net electricity produced annually by the hybrid solar concentrator (E_t) to the thermal energy equivalent of the fuel (natural gas, syngas or biogas) consumed during the same year (Q_t^{fuel}) [48]:

$$PER = \frac{E_t}{Q_t^{fuel}} \left[\frac{kWh_{el}}{kWh_{th}}\right] \tag{5}$$

f. Finally, to quantify the environmental benefits obtained through the two analyzed solar concentration systems, the amount of annual CO_2 emissions avoided (CO_2^{ev}) was calculated using the following equation:

$$CO_2^{ev} = \frac{E_t}{\eta_{grid}} \cdot \mu_{fuel}^{CO_2} \cdot 10^{-3} \left[\frac{t_{CO_2}}{year}\right] \tag{6}$$

where η_{grid} is the average conversion efficiency of the national electricity park (equal to 0.46), $\mu_{fuel}^{CO_2}$ is the CO_2 emission factor of the fossil fuel used to power the hybrid solar concentrator expressed in $kgCO_2/kWh_{th}$.

3. The dish-Stirling plant of UNIPA

In December 2017, the installation of a dish-Stirling plant was completed at the Department of Engineering of the University of Palermo (see Fig. 1). The system was designed and constructed by the Swedish company Ripasso Energy, with installation support from Elettrocostruzioni Srl [49] and Horizon S.r.l [50]. The plant consists of a single production unit with a peak output power of 32 kW and occupies an area of approximately 500 m^2. The key technical data of this plant are summarized in Table 3.

Fig. 1. The UNPA dish-Stirling plant.

The UNIPA dish-Stirling unit comprises a paraboloidal concentrator, a power conversion unit (PCU), and a biaxial tracking system. The concentrator is supported by a lightweight steel structure and consists of 104 mirrors of various sizes arranged in five circles. Each mirror has a double curvature and is constructed using a sandwich structure. The upper surface of the mirror is made of glass, which provides a high reflectivity coefficient of 0.95. This design ensures efficient reflection and concentration of solar radiation onto the receiver, optimizing the overall performance of the system. The PCU, situated at the focal point, consists of a heat receiver with an internal cavity, a Stirling engine, an alternator and a cooling system. The biaxial solar tracking system, equipped with high precision, ensures the concentrator follows the sun's path, allowing for the collection and concentration of direct solar radiation onto the receiver. This tracking system, composed of a steel reticular structure, moves on a track anchored to the concrete foundation. The reflector collects and concentrates the incoming solar beam radiation onto the receiver. Therefore, the thermal energy absorbed by the receiver heats the working fluid of the Stirling engine (hydrogen) to a temperature of about 720 °C. The Stirling engine converts part of this thermal energy into mechanical energy, which is further transformed into electrical energy by a three-phase alternator keyed to the same crankshaft. The remaining heat is dissipated into the environment by the cooling system, maintaining a high-temperature difference between the hot and cold sides of the Stirling engine (720 °C and 70 °C, respectively).

While the Ripasso CSP unit is characterized by numerous innovative and highly efficient technological components, such as the tracking system and the receiver, the core component of the system is the Stirling engine. The efficient Ripasso Stirling engine is an updated version of the original model (USAB 4–95) licensed by Kockums AB in 2008. The engine performance data of the original USAB 4–95 Stirling engine, running at a temperature of 720 °C, can be found in Ref. [51]. The engine has been previously installed in various dish-Stirling models, including MDAC systems in the United States (1984–1985) [52] and SES MPP systems (2008), one of which is located at Sandia National Laboratories in New Mexico, USA [23].

Table 3
Main technical data of the UNPA dish-Stirling plant.

	Description	Value	Unit
Concentrator	Collector diameter.	12	m
	Focal length	7.45	m
	Effective opening area	101	m^2
	Geometric concentration ratio	3217	–
	Reflectivity of clean mirrors	95	%
	Total height during operation	14	m
	Total weight	8000	kg
	Land area occupation	500	m^2
PCU	Stirling engine	Energy storage, double-action cylinders	
	Volume moved	4 x 95	cm^3
	Typical power at DNI = 960 W/m2	31.5 @ 2300 rpm.	kW_e
	Receiver temperature	720	°C
	Working fluid	hydrogen	–
	Max gas pressure	200	bar
	Power control	Pressure-speed control	
	Weight	700	kg

3.1. The energy model of the UNPA dish-Stirling plant

To assess the UNIPA dish-Stirling system performance, an energy model based on the energy balance of the system and calibrated using actual operational data was utilized [53]. The energy balance of the dish-Stirling system allows for the evaluation of energy losses affecting its various components. Table 4 presents the equations necessary to determine the quantities of the system's energy balance, from the input solar power to the concentrator to the thermal power delivered to the Stirling engine. Equation 7 shows that the solar power collected by the concentrator ($\dot{Q}_{sun}$), calculated by multiplying the incident solar beam irradiance (I_b) by the net effective area of the paraboloidal reflector (A_n), does not fully contribute to the energy available at the receiver due to optical and thermal losses. Equation 8 defines the solar power reaching the receiver minus the optical losses ($\dot{Q}_{r,in}$). Optically, various factors must be taken into account, including mirror reflectivity, solar radiation interception errors, receiver cavity absorbance, and mirror soiling, all of which can be evaluated using the optical efficiency coefficient (η_o). Thermally, a portion of the high-temperature thermal energy concentrated at the receiver is dissipated into the environment through convective and radiative heat exchanges ($\dot{Q}_{r,out}$ in Equation 9). Finally, the thermal power supplied from the receiver to the hot side of the Stirling engine ($\dot{Q}_{S,in}$) can be evaluated as a difference between the effective solar power concentrated onto the receiver and overall thermal losses affecting it.

According to the model presented in Ref. [53], the mechanical output power ($\dot{W}_S$) of the Stirling engine can be expressed as a linear function of the high-temperature power heat delivered from the receiver ($\dot{Q}_{S,in}$) to the hydrogen on the hot side of the engine, as shown in the following equation (Equation 7):

$$\dot{W}_S = \left(a_1 \cdot \dot{Q}_{S,in} - a_2\right) \cdot R_T \tag{11}$$

where, a_1 and a_2 are two positive fitting parameters, while R_T is a temperature correction factor, which is calculated as the ratio of the reference ambient air temperature (25 °C) and the actual one, both expressed in Kelvin.

Simultaneously, a portion of low-temperature heat, equal to the difference between the thermal power input into the Stirling engine and the mechanical power produced, is extracted from the cold side of the engine through a cooling system. By knowing the mechanical power available to the Stirling crankshaft, the net electrical output power of the dish-Stirling system can be evaluated, taking into account its mechanical-to-electrical conversion efficiency (η_e). Subsequently, accounting for the electricity consumption of the tracking system and the dry-cooler ($\dot{E}_p$), the net electrical output power of the dish-Stirling system ($\dot{E}_n$) can be determined.

$$\dot{E}_n = \eta_e \cdot \dot{W}_S - \dot{E}_p \tag{12}$$

The energy balance described reveals that the electrical output of the dish-Stirling system is primarily influenced by three parameters: solar beam irradiance, ambient air temperature and mirror cleanliness. This energy model was implemented using Transient System Simulation Tool (TRNSYS - version 17) [54]. Fig. 2 illustrates the diagram depicting the operation of the solar concentrator, incorporating the input efficiency curves constructed based on manufacturer-provided data.

The climate file used in the model is based on Meteonorm7 [45], which provides a generic average meteorological year for a specific location by interpolating experimental data collected with the aid of satellite images. In this case, the climate data for Palermo was obtained from the Falcone-Borsellino airport meteorological station in Punta Raisi (in the province of Palermo). The dish-Stirling energy model aims to quantify energy outputs, both electrical and thermal. To determine the optimal values of the fitting parameters (a_1 and a_2, as described in Equation (11)) of the linear model mentioned earlier, the numerical model of the dish-Stirling system was calibrated using data collected during the actual operation period. The model calibration was performed using clean mirrors and data from days with clear skies. The monitored data included direct normal irradiance (DNI), air temperature, gross electricity produced by the alternator and electricity consumed by the tracking system and the dry-cooler. Once the geometric and optical parameters of the system were set, along with the receiver temperature, the thermal power input to the Stirling engine was calculated, and consequently, the mechanical power produced for each pair of monitored DNI and air temperature values.

The calculated mechanical power values were compared with the real electrical production data of the dish-Stirling system to determine the optimal fitting parameters of the linear relationship. The resulting values were $a_1 = 0.477$ and $a_2 = 3.9$ W. As shown in Fig. 3, the numerical model provides a coefficient of determination of 0.97, allowing for the estimation of the electrical production capability of the dish-Stirling system [53].

3.2. Hybridization of the UNPA dish-Stirling plant

As mentioned earlier, the intermittence and variability of renewable energy sources are their main drawbacks. The electrical producibility of a dish-Stirling solar concentrator primarily relies on direct normal irradiation, which means that the hourly production profile may not align with the electricity demand of the end user. Integrating a hybrid dish-Stirling system would enable more efficient energy utilization by combining two independent systems that can balance their production with the consumer's electricity requirements. The key components of the dish-Stirling solar concentrator - the receiver, the Stirling engine and the electric generator - can operate independently using either solar energy or fuel gas (natural gas, biogas or syngas). Fig. 4 presents a schematic representation of the layout of the dish-Stirling system installation, where the main components required for resource

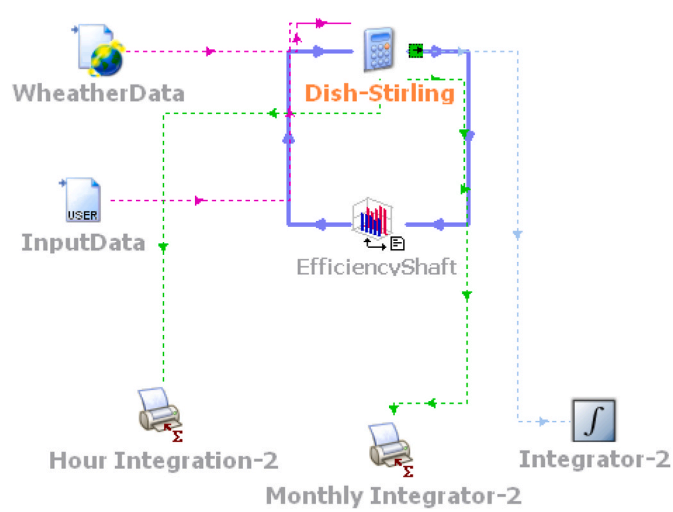

Fig. 2. TRNSYS layout of the UNIPA dish-Stirling plant model.

Table 4
Equations of the energy balance: from solar power to thermal input power of the Stirling engine.

Equation	
$\dot{Q}_{sun} = A_n \cdot I_b$	(7)
$\dot{Q}_{r,in} = \eta_o \cdot \dot{Q}_{sun}$	(8)
$\dot{Q}_{r,out} = A_r \cdot [h_r \cdot (T_r - T_{amb}) + \sigma \cdot \varepsilon \cdot (T_r^4 - T_{sky}^4)]$	(9)
$\dot{Q}_{S,in} = \dot{Q}_{r,in} - \dot{Q}_{r,out}$	(10)

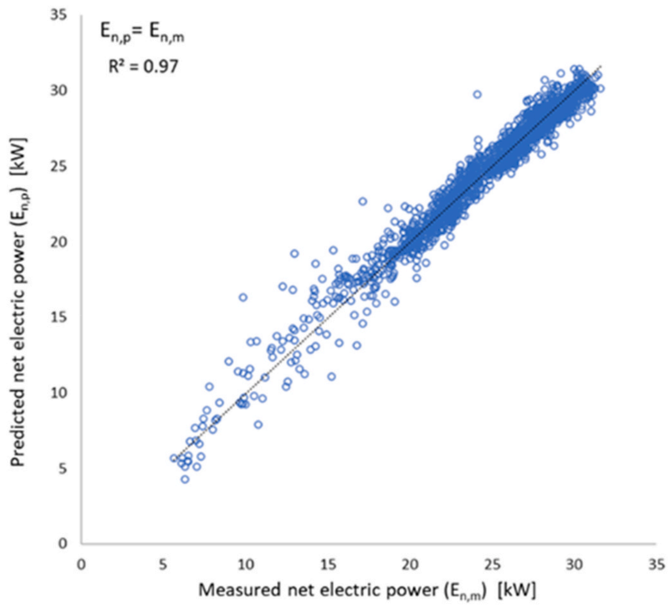

Fig. 3. Net electrical power measured compared to that calculated for the days when the collector mirrors were clean [53].

hybridization can be observed; it is not intended to be a technical diagram. The proposed layout for the hybrid dish-Stirling system includes additional components.

- The fuel supply system, which comprises the necessary pipes and components for transporting the fuel used to the combustion unit.
- The combustion unit, consisting of the combustion chamber, ignition device, fuel regulator, and burner.
- The air supply fan, which serves as the oxidizer in the combustion chamber.
- The heat recovery system, a heat exchanger that preheats the air entering the combustion chamber by utilizing residual heat from the exhaust gases.
- A control system that allows for seamless transition and operation of the dish-Stirling system between solar and hybrid modes.

As shown in the simplified scheme of Fig. 4, the high-temperature exhaust gases, generated in the combustion chamber through the oxidation reaction of the combustible gas with air, flow towards the PCU, transferring thermal energy to the Stirling engine. This process raises the working fluid (hydrogen) to the required temperature and pressure for it to undergo thermodynamic transformation within the Stirling engine, following the Stirling cycle. Following heat exchange in the PCU, the still hot exhaust gases are directed to a heat recovery unit, where they preheat the incoming air in counter-current arrangement. In the hybrid configuration of the dish-Stirling system, the theoretical efficiency of the heat exchange between the combustion products and the hydrogen within the PCU is 80%.

The following hybridization scenarios have been identified for the UNIPA dish-Stirling system.

- Scenario 0: The system operates solely on solar energy.
- Scenario I: The system operates on solar energy during hours with direct solar radiation, while for 12 h per day (from 19:00 to 6:00), alternative sources such as natural gas, syngas, or biogas are utilized throughout the year.
- Scenario II: The system relies on solar energy during hours with direct solar radiation, and for 8 h per day (from 21:00 to 4:00), it uses other sources (natural gas, syngas, or biogas).
- Scenario III: The system uses solar energy during hours with direct solar radiation and employs other sources (natural gas, syngas, or biogas) during daylight hours when the DNI level is lower than or equal to 300 W/m^2.

4. Dish-MGT of ENEA

As previously mentioned, the OMSoP plant, installed and commissioned at the ENEA Casaccia Research Center in 2017, is the demonstration prototype of an innovative concentrating solar technology, based on the use of a circular parabolic concentrator combined with a micro-gas turbine with the aim of experimenting advanced solutions to produce renewable energy from the solar source. The realization of the prototype was funded by the EU OMSoP - Optimized Microturbine Solar Power System project [15]. The main innovation of the project lies in the replacement of the Stirling engine with the MGTs technology derived from the automotive industry, to obtain a more reliable and cost-effective system. The main components of the system, whose conceptual scheme is shown in Fig. 5, are the solar concentrator, the receiver and the Micro Gas Turbine. The solar receiver (cavity type), positioned in correspondence with the focal point of the dish, absorbs the concentrated radiation and transfers it to a compressed air flow, which is then processed by the MGT for producing mechanical work, through a recuperated Brayton cycle, with an operative pressure of 3

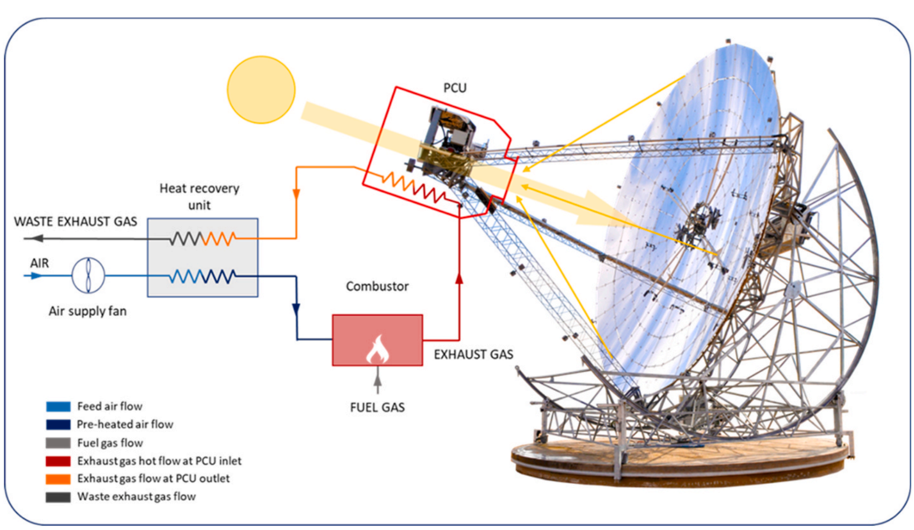

Fig. 4. Plant layout of the hybrid dish-Stirling solar concentrator.

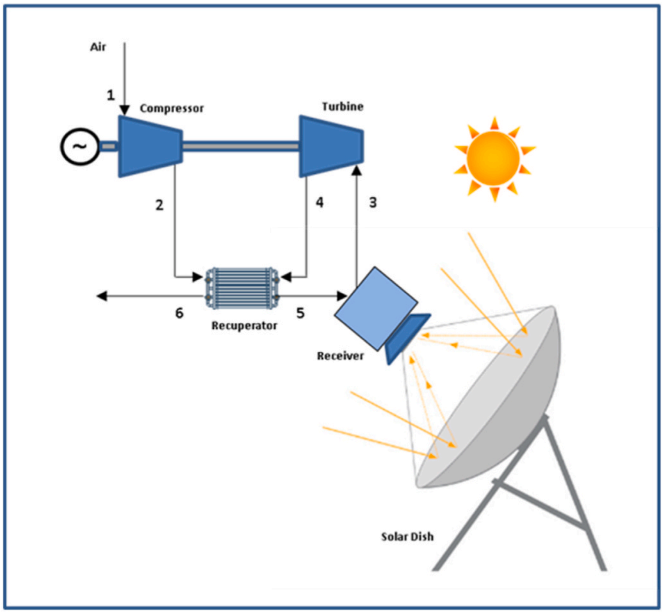

Fig. 5. Conceptual scheme of the gas dish/microturbine technology developed within the OMSoP EU Project.

atm and a maximum temperature of 900 °C.

Particularly, the hot air leaving the receiver (T: 800 °C) is processed in the turbine to produce electricity while the residual heat is transferred to a recuperator for the pre-heating of the external air. The micro-gas turbine is composed of a compressor, which sucks in the external air and compresses it to about 3 atm, and a turbine, mounted on the same shaft, where the air flow at 800 °C expands to produce mechanical work. The expansion in the turbine activates a high-frequency generator that reaches a rotation speed of about 130000 rpm, ensuring a nominal output power of about 6 kW.

As part of this work, a system model describing the OMSoP technology was implemented aimed at predicting the operation of the Dish-MGT (D-MGT) plant in different geographical contexts, both in "full solar" configuration and hybridized with fossil sources. The demo model was assembled trough the integration of different modules, corresponding to the main system components, each represented as a box described by characteristic equations or performance maps. Each component model was separately implemented in EES (Engineering Equation Solver) and then integrated into the whole system through heat and mass balance equations in the TRNSYS environment. The resulting model is a quasi-steady state model and enables the simulation of the plant on a large time scale (annual), determining the performance of the system (electrical power produced, efficiency, capacity factor, etc.) in different atmospheric and operating conditions (both nominal and off-design). The model input data are the DNI and the ambient temperature, whose variability significantly affects the performance of MGT on the annual scale. In the following, the main models implemented for each single component are briefly described.

4.1. Dish

According to the analysis presented in Ref. [55], the flux distribution on the focal plane φ(ξ) can be expressed as a function of the geometry of the parabolic dish, the radius of the receiver window ξ and the error angle θ_S (which takes into account the angle of the solar disk (4.7 mrad), increased by the contributions of the error in the shape of the paraboloid, the imperfect specularity of the mirrors, the diffraction, and the tracking error):

$$\varphi(\xi) = \varphi^{peak}\left(1 - e^{-\frac{\xi^2}{2\mu^2}}\right) \tag{13}$$

with φ^{peak} expressed as

$$\varphi^{peak} = \frac{P_{in}}{2\pi\mu^2} = \frac{\eta_r P_{coll}}{2\pi\mu^2} = \frac{9}{32}\frac{\eta_C DNI}{\left(r_g/D\right)^2} \tag{14}$$

where P_{in} is the power intercepted by the window, η_r is the efficiency of the reflecting surface (reflectance), r_g is the rim angle and P_{coll} is the power collected on the surface of the mirrors. Based on the previous equations, it is possible to predict quite accurately the optical performance of the concentrator (optical efficiency) as a function of the geometry of the dish, the total tracking error and the radius of the receiver. The optical efficiency of the system, defined as the ratio between the power intercepted by the receiver P_w and the power globally collected by the concentrator P_{coll}, can be expressed through the following equation:

$$\eta_{opt} = \frac{P_w}{P_{coll}} = \eta_r\left(1 - e^{-\frac{r^2}{2\mu^2}}\right) \tag{15}$$

with η_r reflectivity of the mirrors.

4.2. Cavity receiver

The cavity receiver has a window radius r equal to 110 mm. The energy reflected and concentrated on the receiver window does not coincide with the useful energy transferred to the air flow due to different heat dissipation mechanisms. In the present work, an apparent absorption coefficient α equal to 0.8 was assumed to take into account the complex phenomena of absorption/reflection [55].

$$\eta_{abs} = \frac{P_{abs}}{P_w} = \alpha \tag{16}$$

where η_{abs} is the absorption efficiency, P_w is the power incident on the receiver window and P_{abs} the power absorbed by the cavity. The power P_{net} transferred to the fluid was calculated on the basis of the following heat balance:

$$P_{net} = P_{abs} - P_{reirr} - P_{conv} = \dot{m}_{air}\cdot(h_3 - h_5) \tag{17}$$

$$P_{reirr} = \varepsilon\cdot\sigma\cdot A_w\left({T_3}^4 - {T_{sky}}^4\right) \tag{18}$$

$$P_{conv} = U_{conv}\cdot A_w\cdot(T_3 - T_a) \tag{19}$$

where P_{reirr} is the power lost by irradiation, ε is the emissivity of the receiver, σ is the Stefan-Boltzmann constant, T_3 is the temperature of the receiver assumed to be homogeneous and equal to the outlet air temperature, T_{sky} is the reference temperature for re-radiation phenomena (15 °C), T_a is the ambient temperature, P_{conv} is the thermal power lost by convection from the window surface, A_w is the window surface, m_{air} is the air flow rate processed in the receiver, h_5 and h_3 are the inlet and outlet specific air enthalpies, U_{conv} is the global heat transfer coefficient used for the calculation of the convective losses from the window surface, obtained from the following correlation [56]:

$$U_{conv} = b\cdot\left(\Delta_{tf}\right)^m L^{3m-1} \tag{20}$$

where b (1.32–1.37) and m (0.25) are empirical parameters that depend on the thermophysical properties of the fluid (air) and the geometry of the system, Δt_f is the temperature difference between the hot surface and the ambient temperature, L is the characteristic dimension of the system. For the calculation of the thermal losses, the natural convection from the external walls of the cavity, which are assumed to be covered by an insulating coating, was neglected.

4.3. Cavity receiver

The performance maps of the turbine and the compressor (Figs. 6 and 7, respectively) were provided by City University within the OMSoP Project [57], while for the HSG (High Sped Generator) a fixed efficiency equal to 0.9 was assumed. In particular, the turbo-compressor operating point was individuated by matching the air flow rate m_{air} and the compressor pressure ratio P_{ratio} and PR (P_{ratio}, net of the cycle pressure drops). Furthermore, since the driving torque and the load torque are perfectly balanced in the steady state condition, the electrical power output Pele is equal to the turbo-compressor net power, as reported in the following relation:

$$P_{ele} = (P_t - P_{cm})\cdot\eta_{ele} \tag{21}$$

where η_{ele} is the electrical efficiency of the HSG, P_t and P_{cm} are the total turbine and the total compressor power, respectively. Concerning the recuperator, it was assumed, as a preliminary approximation, that the heat exchange efficiency η_{rec} has a stepwise behaviour, being 0.85 for a turbine outlet temperature equal to or higher than 160 °C and 0 in correspondence to a temperature lower than 160 °C.

For the MGT integration into the system model, the following heat and mass balance equations have been considered (see Table 5 for the streams notations).

where P_{cm} is the total compressor power, P_c is the power absorbed by the compressor, net of the mechanical efficiency η_{mec}, h is the specific air flow enthalpy, h_{is} is the isentropic air flow enthalpy, η_{cm} and η_t are the compressor and the turbine isentropic efficiencies respectively, η_{rec} is the recuperator effectiveness and P_{rec} is the recuperator power.

4.4. Full solar system

As previously mentioned, through the integration of the modules above described, developed as sub-routines in the EES environment, a complete system model was subsequently implemented, suitable for simulating the operation of dish-MGT, both in nominal and off-design conditions. The main descriptive and operational parameters of the system are shown in Table 6. It is worth noticing that the size of the current dish does not correspond to the OMSoP prototype one [55], which was oversized compared to the MGT's capacity in order to guarantee a good margin of flexibility for the OMSoP research project. In the present study, indeed, the dish size was reduced to perfectly match the MGT's capacity (~6.44 kWe) while maximizing the plant producibility over the year.

The coupling between the micro-gas turbine and the solar source poses the issue of ensuring optimal operation of the system even in off-design operating conditions, i.e. when the DNI and ambient temperature vary. Indeed, the efficiency of Brayton-type thermodynamic cycles is

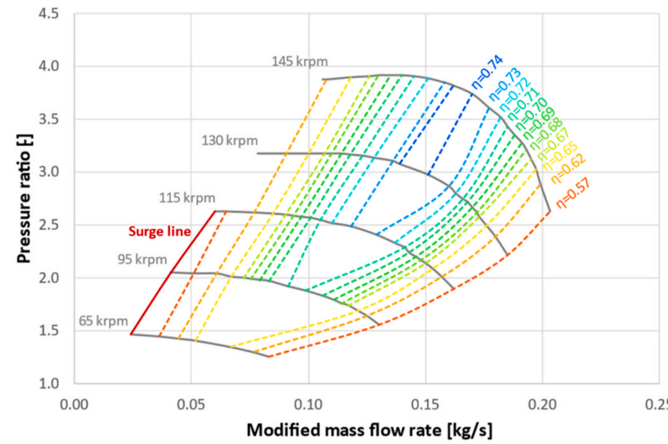

Fig. 7. Compressor performance map [58].

Table 5
Heat and balance equations for the MGT group [15,58].

Compressor		Recuperator		Turbine	
$P_{cm} = \frac{P_c}{\eta_{mec}} = \frac{m_{air} \bullet (h_2 - h_1)}{\eta_{mec}}$	(22)	$P_{rec} = m_{air} \bullet (h_5 - h_2)$	(24)	$P_t = m_{air} \bullet (h_3 - h_4)$	(26)
$\eta_{cm} = \frac{(h_2 - h_1)}{(h_{2is} - h_1)}$	(23)	$\eta_{rec} = \frac{T_5 - T_2}{T_4 - T_2}$	(25)	$\eta_t = \frac{(h_3 - h_4)}{(h_3 - h_{4is})}$	(27)

Table 6
System nominal operating conditions and main component specifications [15,58].

Reference DNI [W/m^2]	720	Receiver pressure drops [%]	1.0
TIT (Turbine Inlet temperature) [°C]	800	Recuperator efficiency [–]	0.81
Dish external diameter [m]	9.9	Recuperator pressure drops [%]	3.4
Dish internal diameter [m]	2.21	Rated speed [krpm]	137
Nominal reflecting area [m^2]	76.7	Air mass flow rate [kg/s]	0.1
Effective reflecting area [m^2]	62.7	Compressor Pressure Ratio [–]	2.4
Mirrors reflectivity [–]	0.92	Compression efficiency [–]	0.74
Total optical error θ_s [mrad]	6.7	Mechanical efficiency [–]	0.99
Global optical efficiency [–]	0.88	Turbine efficiency [–]	0.82
Receiver window diameter [m]	0.22	Generator efficiency [–]	0.90
Receiver thermal efficiency [–]	0.73	Nominal electrical output [kW]	6.44

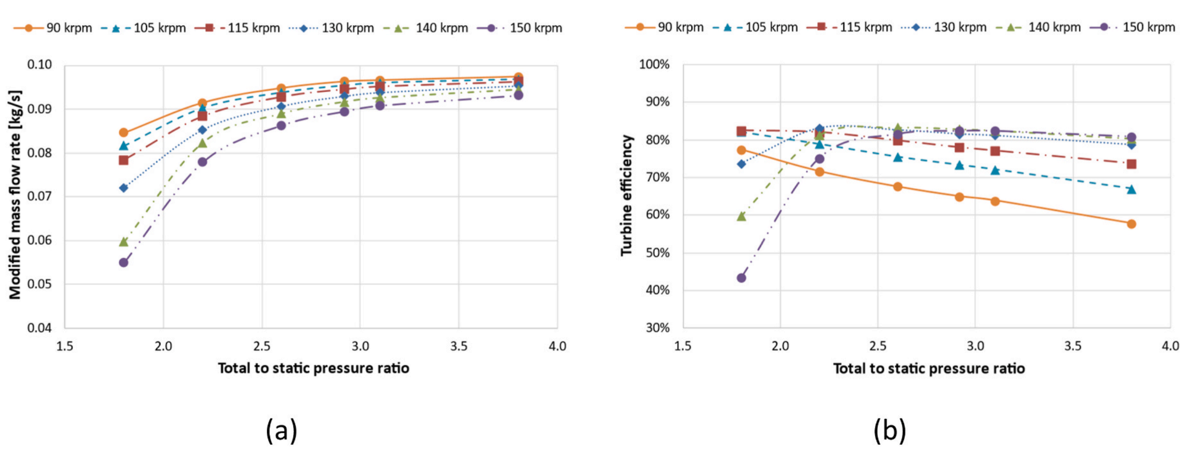

Fig. 6. a) Turbine performance map; b) Turbine efficiency versus pressure ratio [58].

essentially temperature-dependent. In order, therefore, to ensure optimal operation of the system in different environmental conditions, the operating strategy selected for the Dish-MGT system consists in modulating and controlling the air flow to guarantee a constant turbine inlet temperature (800 °C). In practice, this operating strategy requires the definition of a correlation between the MGT speed and the external conditions (ambient temperature and DNI). With this regard, Fig. 8 shows the parametric curves that correlate the MGT speed with the DNI and the turbine inlet temperature (TIT) at constant ambient temperature (25 °C). To maintain the TIT at the nominal value of 800 °C in the different environmental conditions, the MGT must therefore operate following the blue curve in Fig. 8.

By repeating the analysis for different ambient temperatures, it is possible to define the three-dimensional maps of the system performance, through which, by interpolation, the characteristic operating parameters of the system can be identified in all possible combinations of DNI and ambient temperature. These maps were implemented on the TRNSYS code for the evaluation of the annual performance of the Dish-MGT plant in different geographical sites (Casaccia, Marrakesh, Palermo, Ragusa, Tabuk). In Fig. 9 the electrical power produced and the MGT speed in different environmental conditions are shown. The results of the simulations, in terms of annual producibility, solar energy into electricity conversion efficiency, and thermodynamic efficiency of the cycle, are shown in Subsection 3.5.

4.5. Hybridized system

The hybridization of the Dish-MGT system with fossil fuels or biofuels does not require substantial changes to the full solar configuration; indeed it is possible to adopt the solutions conventionally used in the combustor-turbine groups of the automotive sector, suitably revised in terms of size and operational flexibility. In the present work, it was assumed to introduce a combustor sized for the operation between −35% and +35% of the nominal capacity. This combustor can be integrated into the "solar" circuit in different configurations. In particular, starting from the hypothesis of a complete fossil power cycle, in which the combustor replaces the solar receiver and can be positioned both upstream and downstream of the turbine (Fig. 10 a and Fig. 11 a, respectively), at least two main types of hybridized configuration can be conceived: 1) circuit with "internal" combustion (Fig. 10b), in which the combustor is connected in series to the solar receiver and the air flow entering the turbine is heated directly by the combustor (D- MGT-I1); 2) circuit with "external" combustion (Fig. 11b), in which the combustor is integrated downstream of the solar receiver and the air stream entering the turbine is heated through an intermediate heat exchange (D-MGT-I2).

These hybrid configurations correspond to two different hypotheses on the fuel adopted: in the case of the first configuration, in which the combustion effluents are directly processed in the turbine, the use of "clean" fuel gas is required (methane or natural gas), which does not interfere with the chemical and mechanical stability of the materials constituting the body and the blades of the turbine. Clearly, in this specific configuration, the thermal power produced by the combustion is directly absorbed by the air flow and the response time to variable loads is very fast. The second configuration can be considered in the case of renewable fuels, obtained from biological processes and therefore containing different residues and not standardized (e.g., biogas).

Furthermore, in the configurations represented in Fig. 10b) and 11. b) a possible technical solution for connecting the fuel pipe could be the adoption of a flexible pipe connecting the fuel tank, positioned on the ground, to the MGT combustor, positioned on the dish arm.

This flexible tube is intended to pass inside the pole of the dish and, in correspondence with the center of the dish, come out of the pole and be anchored to the arm of the dish until it reaches the container box (and the combustor).

For the modeling purpose, the combustor was assimilated to a black box, where the thermal balance can be expressed through the following relation (combustion efficiency: 97%):

$$P_{fuel} = \dot{m}_{fuel} \cdot LHV \cdot \eta_{cc} \tag{28}$$

where P_{fuel} is the thermal power supplied by the combustor to the air flow, $\dot{m}_{fuel}$ is the fuel flow rate, LHV is the lower heating value of the fuel. The thermal power is transferred to the air flow, as expressed in Eq. (29), which ensures an enthalpy jump in the air flow rate $\dot{m}_{air}$ from, as depicted by Eq. (29):

$$P_{fuel} = \dot{m}_{air} \cdot (h_7 - h_3) \tag{29}$$

where h_3 and h_7 are the specific air enthalpy at the outlet of the receiver and the outlet of the combustor, respectively.

The combustor was integrated into the system model based on the following assumptions.

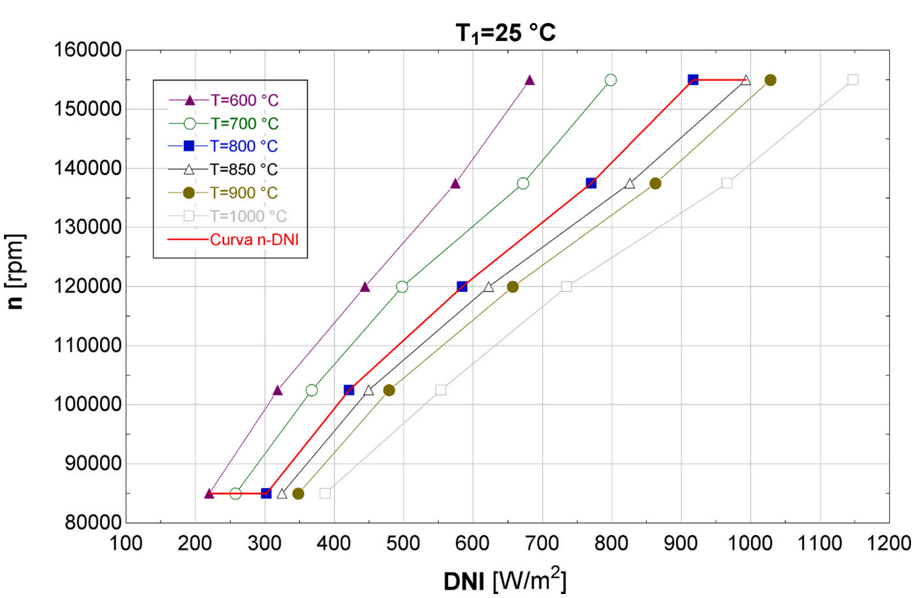

Fig. 8. MGT speed as a function of DNI varying the TIT (Tamb: 25 °C).

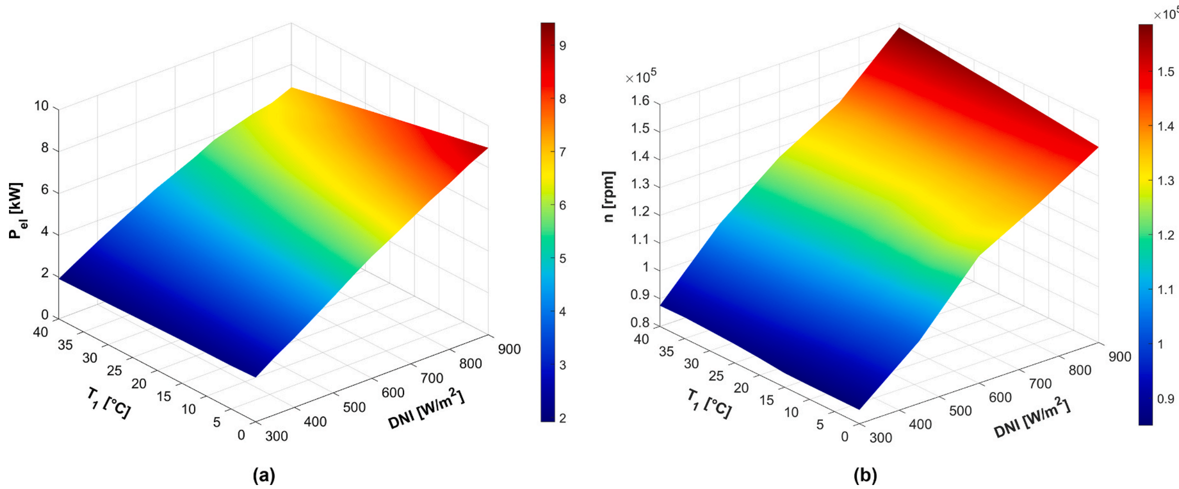

Fig. 9. Performance map of the Dish-MGT system in different environmental conditions (Casaccia site): a) electrical power produced; b) MGT speed.

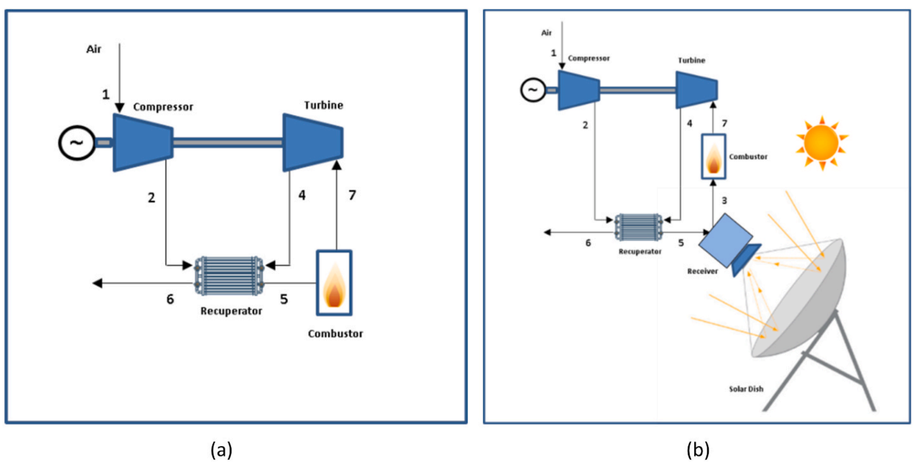

Fig. 10. a) Conceptual scheme of MGT fueled by fossil sources, with combustion "internal" to the cycle; b) Conceptual scheme of dish/MGT technology in the hybridized configuration: case of "internal" combustion (D-MGT-I1).

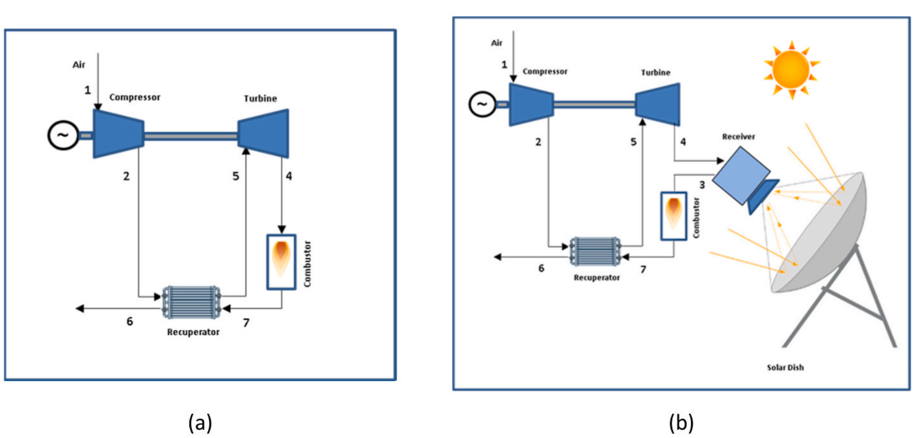

Fig. 11. a) Conceptual scheme of MGT fueled by fossil sources, with combustion "external" to the cycle; b) Conceptual scheme of dish/MGT technology in the hybridized configuration: case of "external" combustion (D-MGT-I2).

- The operation of the combustor is continuous, with a capacity varying between −35% and +35% (to avoid repeated and unrealistic starts and stops daily).
- In nominal conditions, the combustor supplies 40% of the thermal power required by the MGT.
- In Scenario III, the combustor serves to stabilize the electrical output, compensating for fluctuations in the DNI, and is also used in the evening to ensure 24/24 electricity production.

- In Scenario IV the combustor stabilizes and extends the electricity generation in a more profitable time slot (from 7 to 23) in terms of electricity rates applied.

Scenarios I and II, supposed for the dish-Stirling system, have not been analyzed for the Dish-MGT, since they are not economically sustainable, while further hybridization solutions have been considered that aim to better support the deployment of this technology and to reduce the price of electricity production. Indeed, in the case of Scenarios I and II, the combustor and the Dish/receiver should operate in alternating mode, with the Dish/receiver operating only during the day and the combustor only at night. This would involve the adoption of a combustor and a dish individually sized for 100% of the turbine's thermal needs, with a high unit cost of the kWe installed. In the other Scenarios considered, on the contrary, the size of the dish and the receiver are reduced, leading to a lower cost of electricity production. Particularly, in Scenario IV the combustor is meant to stabilize and extend the electricity generation in a more profitable time slot (from 7 to 23) in terms of electricity rates applied.

Fig. 12 shows the representations in the T-s plane of the thermodynamic cycle under nominal conditions for the two hybrid configurations. The comparison shows that the D-MGT-I1 configuration has a higher efficiency since, with the same useful work (represented by segments 7–4 and 5–4), the total thermal power to be supplied (segment 5-3-7) is lower than the D-MGT-I2 configuration (segment 4-3-7). Therefore, for the hybrid configuration D-MGT-I1, it is possible to reduce the size of the solar dish to a diameter of 7.3 m, with a reduction of the reflecting surface of 46% compared to the D-MGT full solar configuration, and to adopt a combustor with a nominal power of 25 kW, thus minimizing the specific cost of the installed kW. On the other hand, for the D-MGT-I2 configuration, the diameter of the solar dish is equal to 8.4 m, with a surface reduction of 28% compared to the full solar configuration, and the combustor has a nominal power of 35 kW.

For the operational strategy, aimed at maintaining constant the electrical output and the TIT through the contribution of the combustor, the manipulated variables are the thermal load of the combustor and the air flow, modulated as a function of the DNI and the environmental temperature.

5. Results and discussion

In this section, the results of the analysis of climatic meteorological data provided by Meteonorm for the five selected locations as potential installation sites will be presented. Subsequently, the results obtained from the annual simulations conducted for both examined parabolic dish systems will be shown: the UNIPA dish-Stirling plant and the ENEA dish-MGT plant.

5.1. The mediterranean climate

The analysis of climatic data plays a crucial role in understanding the environmental characteristics and climatic conditions that impact the performance of parabolic dish solar concentrators. These data provide valuable insights for selecting suitable sites and conducting a comprehensive assessment of the energy system potential. As mentioned in Section 3 "Approach and method", the selected installation locations are distributed across the Mediterranean region and include Casaccia in central Italy for the dish-MGT system by ENEA, Marrakesh in Morocco, Palermo in southern Italy for the dish-Stirling system by UNIPA, Tabuk in Saudi Arabia, and Ragusa in southeastern Italy.

Solar beam radiation and air temperature are key factors influencing concentrator solar power systems. Hourly data were extracted from the typical meteorological year dataset provided by the Meteonorm database for each selected location. The annual direct normal irradiation values were determined, along with the hourly frequency distribution of DNI, to characterize the specific location under consideration. Fig. 13 illustrates these findings, providing valuable insights into the solar resource availability and temporal patterns of solar radiation intensity at the selected site.

Among the Italian cities (Casaccia, Palermo, and Ragusa), Ragusa stands out as having the highest potential for solar electricity generation. It has the highest annual direct solar irradiation value (equal to 2138.3 kWh/m^2/year) and experiences a greater number of hours with high DNI values between 800 and 950 W/m^2 compared to the other two Italian cities considered. The annual hours with DNI values ranging from 800 to 950 W/m^2 are 907, 609, and 497 for Ragusa, Palermo, and Casaccia, respectively. Tabuk, on the other hand, has the highest energy potential overall, with 1911 annual hours of DNI ranging from 800 to 1050 W/m^2, compared to Marrakesh's 1169 h per year. Furthermore, it is noticeable how the average air temperature values decrease corresponding to the DNI classes where the hourly frequency distribution reaches its peak. This can be attributed to the occurrence of clear sky days in the Mediterranean region, which can even take place during the winter season when the external air temperatures are generally lower compared to the rest of the year. The relationship between air temperature and DNI is influenced by various factors, including the intensity of solar radiation and atmospheric conditions. During clear sky days, when there is minimal cloud cover and the direct solar radiation is at its highest, the air temperature tends to be lower due to reduced heat retention by clouds and other atmospheric elements. This leads to lower average air temperature values during periods of higher DNI. Understanding this correlation between DNI and air temperature is crucial for characterizing the climatic conditions and their impact on the performance of solar energy systems in the Mediterranean region.

5.2. Results for UNIPA dish-Stirling plant

Using solar radiation and outdoor air temperature data from the

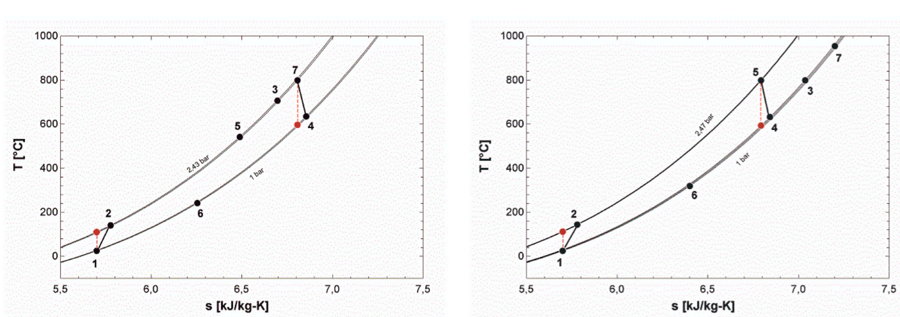

(a) (b)

Fig. 12. Representation of the Brayton cycle for: a) MGT-I1 hybrid configuration and b) MGT-I2 hybrid configuration.

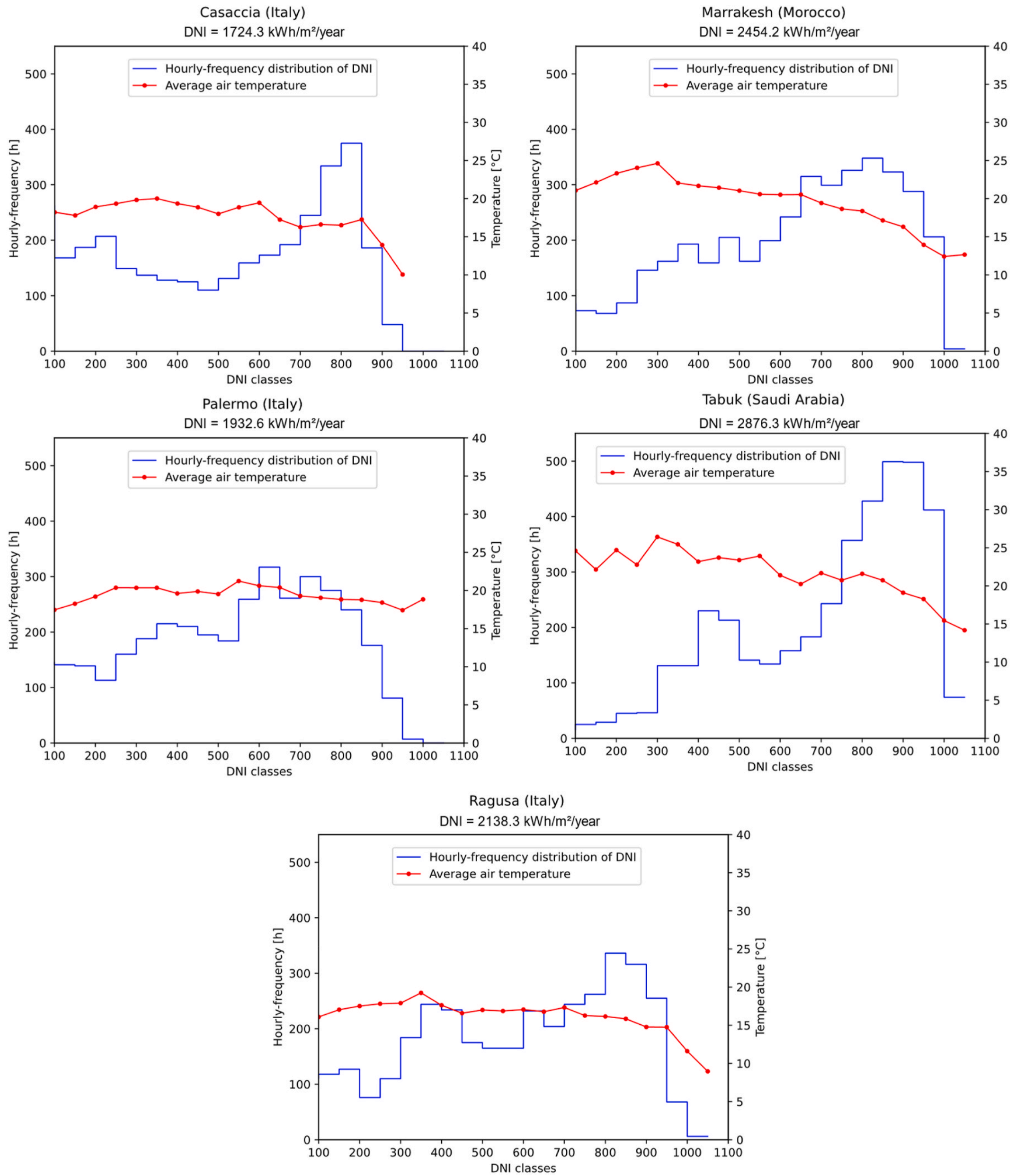

Fig. 13. Hourly-frequency distribution of DNI (bins with a width of 50 W/m^2) and average value and average air temperature values for each bin [45].

Meteonorm database and considering an average annual mirror cleanliness value as described in Section 4.1, the annual electricity production of the UNIPA dish-Stirling system was assessed for various selected locations and hybridization scenarios (see Section 4.2).

Results of the annual simulations demonstrate that the dish-Stirling system achieves a net electricity production of 46 MWh per year in Palermo when solely relying on available solar energy resources (Scenario 0, S_{sh} = 100%). Table 7 highlights that the dish-Stirling solar concentrator in Tabuk surpasses the annual electrical producibility by over 62% (Scenario 0) compared to Palermo. Notably, the simulations indicate that the dish-Stirling system installed in Palermo exhibits the greatest potential for boosting electricity production. By transitioning from Scenario 0 to Scenario III, it achieves an impressive 81% increase in electricity production over the course of a year. Additionally, the solar-electricity conversion efficiency of the same dish-Stirling solar concentrator reaches 22% in Palermo and 25% in Tabuk on an annual basis, as indicated in Table 8.

Table 7
Annual net electrical production of the UNIPA dish-Stirling plant.

E_t [MWh/year]					
	Casaccia	**Marrakesh**	**Palermo**	**Ragusa**	**Tabuk**
Scenario 0	40.5	61.7	46.0	53.3	74.7
Scenario I	186.9	205.7	190.7	199.3	217.7
Scenario II	138.2	157.8	142.5	150.7	170.1
Scenario III	254.7	237.7	239.8	242.9	236.7

Fig. 14a and 14b presented below illustrate the net electrical power

Table 8
Annual solar-to-electricity conversion efficiency of the UNIPA dish-Stirling plant.

$\eta_{sol\text{-}ele}$	Casaccia	Marrakesh	Palermo	Ragusa	Tabuk
Scenario 0	22%	24%	22%	24%	25%

output of the hybrid dish-Stirling system for both a summer day and a winter day, considering all four investigated scenarios. These figures provide valuable insights into the system's performance under different seasonal conditions and emphasize the system's sensitivity to changes in solar resource availability. The DNI values, which represent the intensity of solar radiation received by the dish-Stirling system, vary with the seasons. In winter, due to the lower solar radiation levels, the system's energy production is relatively reduced compared to summer conditions. This difference is evident when examining the net electrical power output curves shown in the figures. Moreover, from these figures, it is evident that the dish-Stirling system efficiently harnesses solar energy during daylight hours, resulting in significant electricity generation. However, during the nighttime hours, the system relies on thermal energy derived from the combustion of natural gas, syngas, or biogas to sustain continuous power generation. In Scenario I, this transition from solar to alternative energy sources occurs between 19:00 and 6:00, while in Scenario II, it takes place between 21:00 and 4:00.

Of particular interest is the observation that when the dish-Stirling system operates according to the guidelines outlined in Scenario III, it ensures continuous electricity production throughout the entire day. By maximizing the utilization of the solar source and strategically switching to alternative energy sources during periods of insufficient solar radiation, Scenario III optimizes the system's performance. These findings demonstrate the versatility and adaptability of the hybrid dish-Stirling system, highlighting its capability to effectively integrate solar and alternative energy sources for sustained electricity generation.

Tables 9 and 10 present the annual mechanical efficiency and thermal efficiency values of the Stirling engine, which vary based on the hybrid concentrator management strategy and location. In Palermo, for Scenario 0, the Stirling engine achieves a thermodynamic efficiency of 39% and a thermal efficiency of 61%. It's worth noting that, in the same location, the hybrid Stirling exhibits a higher thermodynamic efficiency (43%) compared to the solar Stirling engine. This difference arises from the hybrid system operating under peak conditions when powered by energy sources other than solar. Conversely, the thermal efficiency is relatively lower.

Furthermore, S_{sh} index and PER were calculated for all the selected locations to assess the different hybridization scenarios of the dish-Stirling system. The results are presented in Tables 11 and 12. Notably, Tabuk exhibits the highest PER values, aligning with the conversion efficiency values listed in Table 8.

Among the alternative fuels considered for the hybrid dish-Stirling system, natural gas stands out as having the highest LHV value, as shown in Table 1. Additionally, it is the most readily available option if there is no on-site facility for syngas or biogas production. The quantity of natural gas consumed annually for operating the hybrid dish-Stirling system is presented in Table 13, expressed in millions of Nm^3 per year. While the annual natural gas consumption remains constant across

Table 9
Annual Stirling engine thermodynamic efficiency values.

η_M [%]	Casaccia	Marrakesh	Palermo	Ragusa	Tabuk
Scenario 0	38	40	39	40	41
Scenario I	43	43	43	43	43
Scenario II	43	43	42	43	43
Scenario III	44	43	43	44	43

(a)

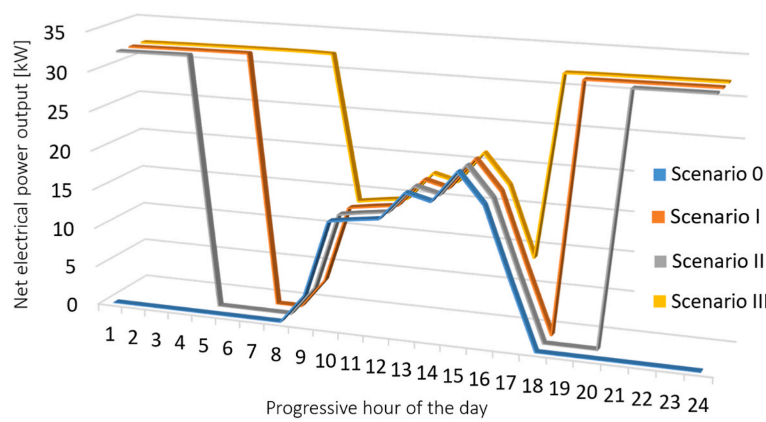

(b)

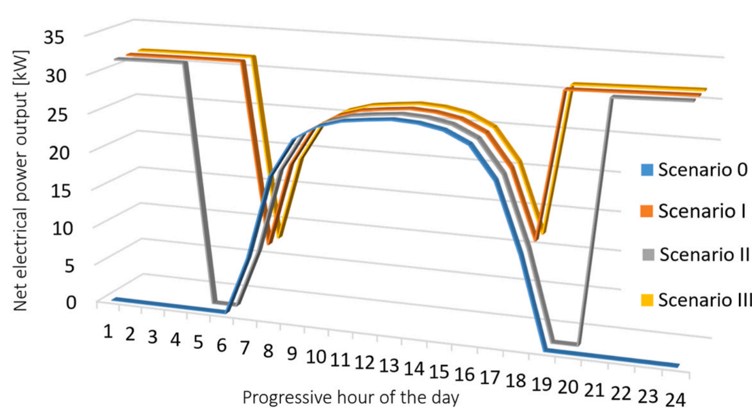

Fig. 14. Net electrical power output of the hybrid dish-Stirling system during a winter day (a) and a summer day (b).

Table 10
Annual Thermal efficiency values of the Stirling engine.

η_T [%]	Casaccia	Marrakesh	Palermo	Ragusa	Tabuk
Scenario 0	62	60	61	60	59
Scenario I	57	57	57	57	57
Scenario II	57	57	58	57	57
Scenario III	56	57	57	56	57

Table 11
Annual solar share values for UNIPA dish-Stirling system.

S_{sh} [%]	Casaccia	Marrakesh	Palermo	Ragusa	Tabuk
Scenario 0	100	100	100	100	100
Scenario I	26	33	28	30	37
Scenario II	34	43	37	39	47
Scenario III	19	29	22	25	34

Table 12
Annual PER values for UNIPA dish-Stirling system.

PER [kWh_{el}/kWh_{th}]	Casaccia	Marrakesh	Palermo	Ragusa	Tabuk
Scenario 0	–	–	–	–	–
Scenario I	0.51	0.56	0.52	0.54	0.59
Scenario II	0.56	0.64	0.58	0.61	0.69
Scenario III	0.47	0.53	0.49	0.51	0.57

different locations for Scenario I and Scenario II, it varies for Scenario III. In Scenario III, the Stirling engine is fueled by thermal energy generated from non-solar sources whenever the DNI level falls below 300 W/m^2. The number of hours with DNI below 300 W/m^2 is lower in Tabuk compared to the other selected Mediterranean locations, resulting in a lower annual natural gas consumption for Tabuk.

Syngas and biogas, despite having lower LHVs compared to natural gas, result in higher annual consumption quantities. To optimize economic viability, it would be beneficial to have a gas production facility near the dish-Stirling system site, exploiting biomass collected in the same vicinity. From an environmental point of view, operating the dish-Stirling system solely on solar energy (Scenario 0) eliminates CO_2 emissions since there is no consumption of natural gas. However, the hybrid dish-Stirling system, operating during the defined hours in Scenarios I, II, and III, emits an annual quantity of CO_2 proportional to the amount of natural gas consumed. Having a syngas or biogas production plant, despite these gases having lower thermal potential, would mitigate CO_2 emissions that would otherwise occur if the Stirling engine were fueled by natural gas combustion. Syngas and biogas are renewable fuels with negligible CO_2 emissions when combusted. The values presented in Table 14 represent both the amount of CO_2 emitted into the atmosphere due to natural gas usage in managing the hybrid dish-Stirling system and the CO_2 emissions avoided by utilizing renewable fuel gases like syngas or biogas.

Considering the possibility of on-site syngas and biogas production,

Table 13
Annual quantity of natural gas consumed for operating the hybrid dish-Stirling system (expressed in millions of Nm^3 per year).

Natural Gas [MNm^3/year]	Casaccia	Marrakesh	Palermo	Ragusa	Tabuk
Scenario I	47.3	47.3	47.3	47.3	47.3
Scenario II	31.5	31.5	31.5	31.5	31.5
Scenario III	69.3	57.6	63.2	61.3	53.2

Table 14
CO_2 emissions avoided through the use of syngas or biogas as an alternative to natural gas.

CO_2^{ev} [tCO_2/year]	Casaccia	Marrakesh	Palermo	Ragusa	Tabuk
Scenario I	87.4	87.4	87.4	87.4	87.4
Scenario II	58.3	58.3	58.3	58.3	58.3
Scenario III	128.0	106.3	116.8	113.2	98.4

if the annual production of these renewable fuels is insufficient to meet the thermal requirements of the hybrid Stirling engine, it may be considered to supplement the power supply of the electricity production plant with natural gas. In relation to this alternative hybridization scenario, it would be valuable to assess the environmental benefit achieved through the reduction of CO_2 emissions compared to the case where the Stirling engine operates solely on thermal energy generated from natural gas combustion. Moreover, it is important to note that the evaluations of the hybridization scenarios focus solely on the replacement of the solar source with one of the three aforementioned gases, without considering the associated costs of gas procurement and transportation.

5.3. Results for dish-MGT plant of ENEA

Based on the system model presented in the previous paragraphs, the performance analysis of the Dish-MGT technology was carried out both in full-solar and hybrid mode in the different locations considered. In particular, the following scenarios were analyzed.

- Scenario 0: the D-MGT system is fully powered by the solar energy source.
- Scenario III: the D-MGT system is co-powered by the solar source and by the combustion of natural gas, syngas, or biogas during the day, with a solar share in nominal conditions equal to 60%. During the night the system is powered exclusively by the combustor. Both hybridized configurations 1 and 2 were considered.
- Scenario IV: the D-MGT system is co-powered by the solar source and by the combustion of natural gas, syngas, or biogas in the 7 a.m.-11 p.m. time slot, with a solar share in nominal conditions equal to 60%. Both hybridized configurations 1 and 2 were considered.

From the results of the annual simulations of the full solar Dish-MGT technology (reported in Table 15), it is possible to observe how the annual electricity production strictly depends on the plant location and is favoured by the sites with the highest solar irradiation. The best performance is obtained for the Marrakesh plant, with a 23% higher producibility compared to the Casaccia site. It is worth noticing that, since the Dish-MGT system was designed and sized for the Casaccia site, in sites characterized by higher solar irradiations, it is sometimes necessary to defocus the system. For this reason, in Tabuk, a lower producibility is obtained compared to Marrakesh, as the defocusing time is longer. Therefore, a specific sizing of the D-MGT system for each site is necessary to optimize the annual electricity production. Regarding the solar-electricity conversion efficiency on a yearly basis, it ranges from 13.6 to 14.0%, as shown in Table 16.

Table 15
Annual electrical producibility values for the Dish/MGT system.

E_t [MWh/y]	Casaccia	Marrakesh	Palermo	Ragusa	Tabuk
Scenario 0	13.1	16.1	14.9	15.3	15.4
MGT-I1 - Scenario III	56.4	56.4	56.4	56.4	56.4
MGT-I1 - Scenario IV	37.6	37.6	37.6	37.6	37.6
MGT-I2 - Scenario III	50.1	52.8	52.6	50.5	52.9
MGT-I2 - Scenario IV	34.2	35.8	35.5	34.4	35.9

Table 16
Annual solar-electricity conversion efficiency for the Dish/MGT system.

$\eta_{sol\text{-}ele}$ [%]	Casaccia	Marrakesh	Palermo	Ragusa	Tabuk
Scenario 0	14.0	13.7	13.8	13.9	13.6

Referring to the hybrid configuration D-MGT-I1 and Scenario III, Fig. 15 shows the thermal power supplied by the combustor and the thermal power from the solar source on a typical sunny summer day and a representative winter cloudy one, respectively, in Fig. 15a and Fig. 15b. In the first case, it is possible to collect thermal power primarily from the solar source in the timeframe 8–18, with the combustor contributing very little during these hours while working at full load during the night. On the contrary, on a cloudy winter day, it is necessary for the combustor to operate throughout the day at full capacity and, only in correspondence of DNI higher than 300 W/m^2, the power required from the combustor decreases with a consequent reduction in the use of fossil fuel.

Comparing the electrical output of the full solar and hybrid D-MGT systems shown in Tables 15 and it can be observed that the hybrid configuration D-MGT-I1 (with "internal" combustion) is able to guarantee a constant electrical output, regardless of the installation site. The D-MGT-I2 system (with "external" combustion) is characterized by limited performances since on average the producibility is 10% lower than the D-MGT-I1 solution. Table 17 shows the thermodynamic efficiency of the MGT calculated yearly: for the full solar system and the D-MGT-I1 hybrid system, the efficiency is approximately 24%, while for the D-MGT-I2 system, it drops to 15%. However, it is important to underline that, in an optimized configuration of the cycle, i.e. in the presence of inter-refrigerated compression and reheating, the thermodynamic efficiency of the cycle can be increased up to 30%, bringing the overall solar-electricity conversion efficiency up to 20%.

Table 18 and Table 19 show the Ssh and PER calculated on a yearly basis, respectively, for the different hybridization scenarios and different sites considered. The best performance for each system is obtained in Tabuk.

Table 20 shows the amount of natural gas, expressed in Nm^3/y, consumed for the operation of the hybrid D-MGT systems. The D-MGT-I1 system, being more efficient, consumes a lower amount of fuel. For both hybrid solutions, Scenario IV has lower fuel consumption, not only due to the lower operating hours (from 7 to 23 compared to the 24 h of Scenario III) but also due to the higher solar share.

Finally, Table 21 shows the CO_2 emissions associated with the use of natural gas in the hybrid D-MGT systems. Regarding the environmental impact, obviously, the operation of the full solar D-MGT system (Scenario 0) does not involve CO_2 emissions. On the contrary, hybrid systems in Scenarios III and IV emit a quantity of CO_2 proportional to the amount of natural gas consumed. If biogas was used as an alternative to natural gas, CO_2 emissions could be considered null, and Table 21 could be read in terms of avoided CO_2 emissions.

6. Conclusions

Parabolic dish collectors offer promising potential for supporting the decarbonization process and reducing fossil fuel consumption in buildings and industries. Compared to photovoltaic panels, these concentrators provide advantages such as combined heat and power generation, flexible electricity production through thermal energy storage, and easy integration with other energy sources for increased annual production. Among CSP technologies, parabolic dish systems stand out due to their higher solar-to-electricity conversion efficiency, modularity, and sustainability for off-grid installation.

In this study, a numerical analysis was carried out using TRNSYS to estimate the annual energy production of two small-scale parabolic dish systems: the dish-Stirling system at the University of Palermo and the dish-Micro Gas Turbine system at the ENEA site in Casaccia, Rome. Parametric analysis was performed for five different locations (Casaccia, Palermo, Ragusa, Marrakesh, Tabuk) with varying levels of direct normal irradiance, and the results were compared. It was extensively investigated the possibility of hybridizing the power conversion units of the two dish systems with fossil fuels (natural gas) or renewable energies (syngas, biogas) to enhance system efficiency and optimize plant, thus improving electricity production stability. The performances of the systems under four scenarios, characterized by different levels of hybridization and operating hours, were evaluated numerically.

The key results of this study are as follows.

- The dish-Stirling system powered solely by solar energy achieves maximum electricity production in Tabuk, reaching 75 MWh per year, which is more than 62% higher than the performance in Palermo due to the higher availability of DNI. The annual solar-to-electricity conversion efficiency of the UNIPA dish-Stirling system is 22% in Palermo and 25% in Tabuk.
- To extend the operational period and increase the power generation of the dish-Stirling system, the integration of an external combustor to burn natural gas or syngas/biogas derived from agricultural residues was evaluated. This integration allows for an 81% increase in electricity production in Palermo.
- The ENEA dish-MGT system achieves maximum power production in Marrakesh, as opposed to Tabuk, where the system experiences a longer period of mirror defocusing. This difference is due to the original system design based on the DNI characteristics of the

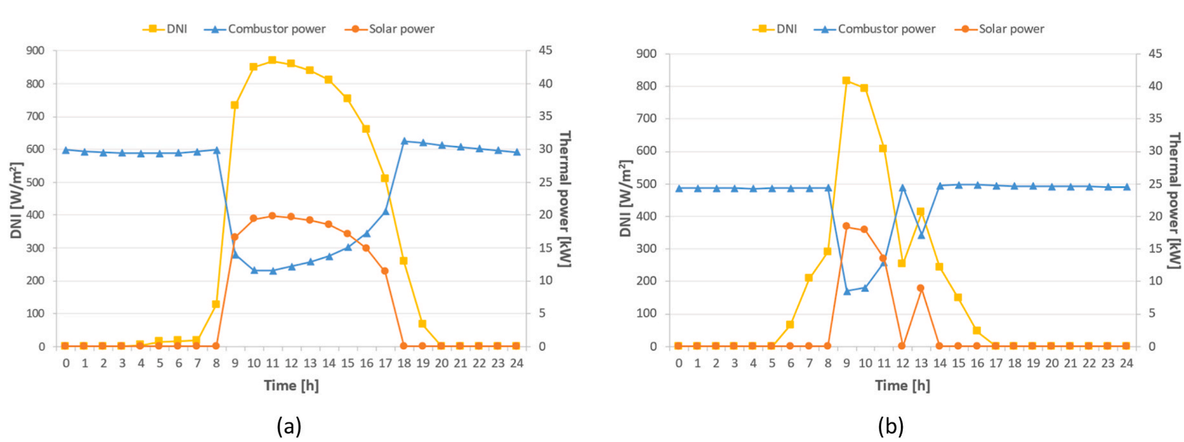

Fig. 15. Thermal power supplied by the combustor and by the concentrating solar system in the case of the hybrid configuration MGT-I1 - Scenario III, in a typical summer sunny day (a) and in a representative winter cloudy day (b).

Table 17
Thermodynamic efficiency of the Micro Gas Turbine on a yearly basis.

η_M [%]	Casaccia	Marrakesh	Palermo	Ragusa	Tabuk
Scenario 0	24.4	24.0	24.3	24.4	23.6
MGT-I1 - Scenario III	24.8	24.3	24.6	24.9	24.0
MGT-I1 - Scenario IV	24.6	24.0	24.5	24.7	23.6
MGT-I2 - Scenario III	14.6	15.6	15.5	14.7	15.8
MGT-I2 - Scenario IV	15.1	16.0	15.8	15.1	16.0

Table 18
Solar share on a yearly basis for the Dish-MGT systems considered.

S_{sh} [%]	Casaccia	Marrakesh	Palermo	Ragusa	Tabuk
Scenario 0	100	100	100	100	100
MGT-I1 - Scenario III	13.8	20.7	15.9	18.2	24.6
MGT-I1 - Scenario IV	20.3	30.7	23.5	26.9	36.4
MGT-I2 - Scenario III	11.5	14.6	13.2	13.1	14.9
MGT-I2 - Scenario IV	17.2	22.0	19.8	19.6	22.3

Table 19
Primary Energy Ratio on the annual basis for the Dish/MGT systems considered.

PER [kWh_{el}/kWh_{th}]	Casaccia	Marrakesh	Palermo	Ragusa	Tabuk
Scenario 0	–	–	–	–	–
MGT-I1 - Scenario III	0.25	0.27	0.26	0.27	0.28
MGT-I1 - Scenario IV	0.27	0.30	0.28	0.29	0.32
MGT-I2 - Scenario III	0.14	0.16	0.16	0.15	0.16
MGT-I2 - Scenario IV	0.16	0.18	0.17	0.16	0.18

Table 20
Natural gas consumed on a yearly basis for the operation of hybrid Dish-MGT systems (expressed in thousands of Nm^3 per year).

Natural gas [kNm^3/year]	Casaccia	Marrakesh	Palermo	Ragusa	Tabuk
MGT-I1 - Scenario III	23.1	21.6	22.7	21.8	20.9
MGT-I1 - Scenario IV	14.5	12.7	13.9	13.3	11.9
MGT-I2 - Scenario III	35.6	34.0	34.6	35.1	33.6
MGT-I2 - Scenario IV	22.3	20.6	21.4	21.8	20.5

Table 21
CO_2 emissions associated with the use of natural gas or avoided through the use of biogas for the Dish/MGT systems.

CO_2^{ev} [tCO_2/year]	Casaccia	Marrakesh	Palermo	Ragusa	Tabuk
MGT-I1 - Scenario III	23.3	23.3	23.3	23.3	23.3
MGT-I1 - Scenario IV	15.5	15.5	15.5	15.5	15.5
MGT-I2 - Scenario III	20.7	21.8	21.7	20.9	21.9
MGT-I2 - Scenario IV	14.1	14.8	14.7	14.2	14.8

Casaccia site. The peak solar-to-electricity conversion efficiency of the dish-MGT system is 14%, but it is expected to exceed 20% after appropriate design modifications.

- The integration of an internal combustor fueled by natural gas (D-MGT-I1) or an external combustor fueled by biogas (D-MGT-I2) was evaluated using combustors commonly integrated with gas turbines in the energy or automotive sectors. Through numerical analysis, it was found that the D-MGT-I1 configuration provides stable electricity production regardless of the installation site and is 10% more efficient than D-MGT-I2. The maximum solar share is achieved in the Tabuk site, at 24.6% and 36.4% for 24-h operation and from 7 a.m. to 11 p.m., respectively.

The study demonstrates that hybridizing parabolic dish systems with conventional fuels or other renewable energy sources significantly improves their performance by increasing the number of operational hours and enhancing energy production. These numerical results encourage further refinements and indicate a reliable path for development. Future studies are needed to optimize the economic configuration of these systems.

CRediT authorship contribution statement

Giuseppina Ciulla: Conceptualization, Methodology, Writing – original draft, Writing – review & editing, Supervision. **Stefania Guarino:** Validation, Formal analysis, Investigation, Data curation, Writing – original draft, Writing – review & editing. **Michela Lanchi:** Conceptualization, Data curation, Writing – original draft, Writing – review & editing. **Marco D'Auria:** Validation, Investigation, Writing – original draft, Writing – review & editing. **Maurizio De Lucia:** Supervision, Conceptualization. **Michele Salvestroni:** Software, Formal analysis. **Vincenzo Di Dio:** Supervision, Visualization.

Declaration of competing interest

The authors declare that they have no known competing financial interests or personal relationships that could have appeared to influence the work reported in this paper.

Data availability

Data will be made available on request.

Acknowledgment

"The work is part of the Research and Innovation Project "Solargrid: Sistemi sOlari termodinamici e fotovoLtaici con Accumulo peR co-GeneRazIone e flessibilità Di rete "—cod. ARS01_00532. The project has been jointly funded by the European Union and Italian Research and University Ministry (MIUR) under the Programma Operativo Nazionale "Ricerca e Innovazione" 2014–2020 (PON "R&I" 2014–020)".

Nomenclature

Symbols

a_1, a_2	fitting parameters of the dish-Stirling system numerical model [-; W]
A_n	net area of the reflector of the dish-Stirling system [m^2]
A_r	aperture area of the cavity receiver of the dish-Stirling system [m^2]
A_w	window surface of the cavity receiver of the dish-MGT system [m^2]
b, m	empirical parameters for the calculation of the convective losses from the window surface of the cavity receiver of the dish-MGT system [−]
CO_2^{ev}	amount of annual CO_2 emissions avoided [t_{CO2}/year]

DNI_i hourly direct solar irradiance [W/m^2]
E_i net electricity produced in the i-th progressive hour of the year [MWh]
$\dot{E}_n$ net electrical output power of the dish-Stirling system [kW]
$\dot{E}_p$parasitic electricity consumption of the dish-Stirling system [kW]E_t parasitic electricity consumption of the dish-Stirling system [kW]$E_t$annual electricity production [MWh/year]
h specific air flow enthalpy of dish-MGT system [kJ/kg]
h_{is} isentropic air flow enthalpy of dish-MGT system [kJ/kg]
$h_r$convective heat transfer coefficient at receiver of the dish-Stirling system [W/(m^2•K)]$I_b$solar beam irradiance [W/m^2]L convective heat transfer coefficient at receiver of the dish-Stirling system [W/(m^2•K)]$I_b$solar beam irradiance [W/m^2]Lcharacteristic dimension of the receiver of the dish-MGT system [m]
$\dot{m}_{air}$air flow rate processed in the receiver of the dish-MGT system [kg/s]$\dot{m}_{fuel}$fuel flow rate of the dish-MGT system [kg/s]P_{abs} air flow rate processed in the receiver of the dish-MGT system [kg/s]$\dot{m}_{fuel}$fuel flow rate of the dish-MGT system [kg/s]P_{abs}power absorbed by the cavity receiver of dish-MGT system [kW]
P_c power absorbed by the compressor of the dish-MGT system receiver [kW]
P_{cm} total compressor power of the dish-MGT system [kW]
P_{coll} power collected on the surface of the mirrors of the dish-MGT system [kW]
P_{conv} thermal power lost by convection from the window surface cavity receiver of the dish-MGT system [kW]
P_{ele} electrical output power of the dish-MGT system [kW]
P_{fuel} thermal power supplied by the combustor to the air flow in the dish-MGT system receiver [kW]Fi
P_{in} power intercepted by the window of the dish-MGT system receiver [kW]
P_{net} power transferred to the working fluid of the dish-MGT system [kW]
P_R turbine expansion ratio of the dish-MGT system
P_{rec} recuperator power of the dish-MGT system [kW]
P_{reirr} power lost by irradiation at cavity receiver of the dish-MGT system [kW]
P_{ratio} compressor pressure ratio of the dish-MGT system
P_t total turbine power of the dish-MGT system [kW]
P_w power intercepted by the receiver of the dish-MGT system [kW]
$\dot{Q}_{r,in}$thermal input power of the receiver of the dish-Stirling system [kW]$\dot{Q}_{r,out}$thermal output power of the receiver of the dish-Stirling system [kW]Q_s thermal input power of the receiver of the dish-Stirling system [kW]$\dot{Q}_{r,out}$thermal output power of the receiver of the dish-Stirling system [kW]$Q_s$high-temperature thermal input energy of the Stirling engine [kWh]
$\dot{Q}_{S,in}$thermal input power of the Stirling engine [kW]$Q_{s,in}$ thermal input power of the Stirling engine [kW]$Q_{s,in}$energy supplied by the hydrogen receiver [kWh]
$\dot{Q}_{sun}$solar power collected by the concentrator of the dish-Stirling system [kW]Q_t^{fuel}thermal energy equivalent of the fuel consumed during the year [kWh$_{th}$]r_g solar power collected by the concentrator of the dish-Stirling system [kW]Q_t^{fuel}thermal energy equivalent of the fuel consumed during the year [kWh$_{th}$]$r_g$rim angle of reflecting surface of the dish-MGT system
$R_T$temperature correction factor [−]T_a temperature correction factor [−]$T_a$ambient temperature [°C]
T_{amb}external air temperature [K]$T_r$temperature of the receiver of the dish-Stirling system [K]T_{sky} external air temperature [K]$T_r$temperature of the receiver of the dish-Stirling system [K]T_{sky}reference temperature for re-radiation phenomena (15 °C)
U_{conv} global heat transfer coefficient of the dish-MGT system cavity receiver [W/(m^2•°C)]
$\dot{W}_S$mechanical output power of the Stirling engine [kW]W_S mechanical output power of the Stirling engine [kW]$W_S$mechanical energy produced by the engine [kWh]

Greek letters
α absorption coefficient of the dish-MGT system cavity receiver [%]
Δt_f temperature difference between the hot surface of the dish-MGT system cavity receiver and the ambient temperature [°C]
εemissivity of the receiver [%]η_{abs}absorption efficiency of the dish-MGT system cavity receiver [%]η_{cc} emissivity of the receiver [%]η_{abs}absorption efficiency of the dish-MGT system cavity receiver [%]η_{cc}compressor efficiency of the dish-MGT system [%]
η_{cm}compressor efficiency of the dish-MGT system [%]η_e compressor efficiency of the dish-MGT system [%]$\eta_e$mechanical-to-electrical conversion efficiency of the alternator of the dish-Stirling system [%]
η_{ele} electrical efficiency of the high-speed generator of the dish-MGT system [%]
η_{grid}average conversion efficiency of the national electricity park [%]$\eta_o$optical efficiency coefficient of the dish-Stirling system [%]η_{opt}optical efficiency of the dish-MGT system [%]η_{mec} average conversion efficiency of the national electricity park [%]$\eta_o$optical efficiency coefficient of the dish-Stirling system [%]η_{opt}optical efficiency of the dish-MGT system [%]η_{mec}mechanical efficiency of the dish-MGT system [%]
η_M thermodynamic efficiency of the cycle [%]
$\eta_r$efficiency of the reflecting surface of the dish-MGT system [%]η_{rec}heat exchange efficiency of the dish-MGT system receiver [%]$\eta_{sol-ele}$solar-to-electricity conversion efficiency [%]$\eta_t$turbine isentropic efficiency of the dish-MGT system [%]η_T efficiency of the reflecting surface of the dish-MGT system [%]η_{rec}heat exchange efficiency of the dish-MGT system receiver [%]$\eta_{sol-ele}$solar-to-electricity conversion efficiency [%]η_t turbine isentropic efficiency of the dish-MGT system [%]$\eta_T$thermal efficiency of the engine [%]
$\mu_{fuel}^{CO_2}$$CO_2$ emission factor of the fossil fuel [kgCO_2/kWh$_{th}$]θ_S CO_2 emission factor of the fossil fuel [kgCO_2/kWh$_{th}$]$\theta_S$error angle [mrad]
ξradius of the receiver window of the dish-MGT system [m^2]σ radius of the receiver window of the dish-MGT system [m^2]σStefan-Boltzmann constant, 5.67·10^{-8} W/m^{2}K^4

$\varphi(\xi)$flux distribution on the focal plane of the dish-MGT system [W/m^2]Abbreviations

CH_4	Methane
CO_2	Carbon dioxide
CSP	Concentrator Solar Power
D-MGT	Dish- Micro Gas Turbine
DNI	Direct Normal Irradiance [W/m^2]
EES	Engineering Equation Solver
HSG	High Sped Generator
LHV	Lower heating value Value of the fuel [MJ/Nm^3]
MGT	Micro Gas Turbine
OMSoP	Optimized Microturbine Solar Power System project
PCU	Power Conversion Unit
PER	Primary Energy Ratio
PR	Pressure Ratio
PV	Photovoltaic
TIT	Turbine Inlet Temperature
TRNSYS	Transient System Simulation Tool
UNIPA	University of Palermo

References

[1] M.A. Javadi, M.H. Ahmadi, M. Khalaji, Exergetic, economic, and environmental analyses of combined cooling and power plants with parabolic solar collector, Environ. Prog. Sustain. Energy 39 (2020), e13322, https://doi.org/10.1002/ep.13322.

[2] A.M. Manokar, D.P. Winston, A.E. Kabeel, R. Sathyamurthy, Sustainable fresh water and power production by integrating PV panel in inclined solar still, J. Clean. Prod. 172 (2018) 2711–2719, https://doi.org/10.1016/j.jclepro.2017.11.140.

[3] A. Zendehboudi, M.A. Baseer, R. Saidur, Application of support vector machine models for forecasting solar and wind energy resources: a review, J. Clean. Prod. 199 (2018) 272–285, https://doi.org/10.1016/j.jclepro.2018.07.164.

[4] O. Achkari, A. El Fadar, Latest developments on TES and CSP technologies – energy and environmental issues, applications and research trends, Appl. Therm. Eng. 167 (2020), 114806, https://doi.org/10.1016/j.applthermaleng.2019.114806.

[5] S.S. Kamble, A. Gunasekaran, S.A. Gawankar, Sustainable Industry 4.0 framework: a systematic literature review identifying the current trends and future perspectives, Process Saf Environ Prot 117 (2018) 408–425, https://doi.org/10.1016/j.psep.2018.05.009.

[6] C.P. Kiefer, P. del Rio, Analysing the barriers and drivers to concentrating solar power in the European Union. Policy implications, J. Clean. Prod. 251 (2020), 119400, https://doi.org/10.1016/j.jclepro.2019.119400.

[7] R. Ling-zhi, Z. Xin-gang, Z. Yu-zhuo, L. Yan-bin, The economic performance of concentrated solar power industry in China, J. Clean. Prod. 205 (2018) 799–813, https://doi.org/10.1016/j.jclepro.2018.09.110.

[8] M. Chafie, M.F. Ben Aissa, A. Guizani, Energetic end exergetic performance of a parabolic trough collector receiver: an experimental study, J. Clean. Prod. 171 (2018) 285–296, https://doi.org/10.1016/j.jclepro.2017.10.012.

[9] N. Mahlangu, G.A. Thopil, Life cycle analysis of external costs of a parabolic trough Concentrated Solar Power plant, J. Clean. Prod. 195 (2018) 32–43, https://doi.org/10.1016/j.jclepro.2018.05.187.

[10] K. Mohammadi, M. Saghafifar, K. Ellingwood, K. Powell, Hybrid concentrated solar power (CSP)-desalination systems: a review, Desalination 468 (2019), 114083, https://doi.org/10.1016/j.desal.2019.114083.

[11] K. Rashid, K. Mohammadi, K. Powell, Dynamic simulation and techno-economic analysis of a concentrated solar power (CSP) plant hybridized with both thermal energy storage and natural gas, J. Clean. Prod. 248 (2020), 119193, https://doi.org/10.1016/j.jclepro.2019.119193.

[12] W.D. Stine, RB Diver, A compendium of solar dish/Stirling technology. United States: N. p, 1994, https://doi.org/10.2172/10130410. Web.

[13] T. Mancini, P. Heller, B. Butler, B. Osborn, W. Schiel, V. Goldberg, et al., Dish-stirling systems: an overview of development and status, J Sol Energy Eng Trans ASME 125 (2003) 135–151, https://doi.org/10.1115/1.1562634.

[14] W. Schiel, T. Keck, Chapter 9 - parabolic dish concentrating solar power systems, in: K. Lovegrove, W. Stein (Eds.), Conc. Sol. Power Technol, second ed. second ed., Woodhead Publishing, 2021, pp. 311–355, https://doi.org/10.1016/B978-0-12-819970-1.00007-4.

[15] M. Lanchi, M. Montecchi, T. Crescenzi, D. Mele, A. Miliozzi, V. Russo, et al., Investigation into the coupling of micro gas turbines with CSP technology: OMSoP project, Energy Proc. 69 (2015) 1317–1326, https://doi.org/10.1016/j.egypro.2015.03.146.

[16] S. Semprini, D. Sanchez, A. De Pascale, Performance analysis of a micro gas turbine and solar dish integrated system under different solar-only and hybrid operating conditions, Sol. Energy 132 (2016) 279–293, https://doi.org/10.1016/j.solener.2016.03.012.

[17] M. Liu, N.H. Steven Tay, S. Bell, M. Belusko, R. Jacob, G. Will, et al., Review on concentrating solar power plants and new developments in high temperature thermal energy storage technologies, Renew. Sustain. Energy Rev. 53 (2016) 1411–1432, https://doi.org/10.1016/j.rser.2015.09.026.

[18] L.G. Pheng, R. Affandi, M.R. Ab Ghani, C.K. Gan, Z. Jano, T. Sutikno, A review of Parabolic Dish-Stirling Engine System based on concentrating solar power, Telkomnika 12 (2014) 1142.

[19] V. Siva Reddy, S.C. Kaushik, S.K. Tyagi, Exergetic analysis and performance evaluation of parabolic dish Stirling engine solar power plant, Int. J. Energy Res. 37 (2013) 1287–1301, https://doi.org/10.1002/er.2926.

[20] W. Reinalter, S. Ulmer, P. Heller, T. Rauch, J.M. Gineste, A. Fernere, et al., Detailed performance analysis of a 10kW dish/stirling system, American Society of Mechanical Engineers Digital Collection, in: J. Sol. Energy Eng. Trans. ASME, vol. 130, 2008, 0110131–6, https://doi.org/10.1115/1.2807191.

[21] J. Yan, Y.D. Peng, Z.R. Cheng, F.M. Liu, X.H. Tang, Design and implementation of a 38 kW dish-Stirling concentrated solar power system, in: IOP Conf. Ser. Earth Environ. Sci., vol. 93, 2017, 12052, https://doi.org/10.1088/1755-1315/93/1/012052. Institute of Physics Publishing.

[22] J. Coventry, C. Andraka, Dish systems for CSP, Sol. Energy 152 (2017) 140–170, https://doi.org/10.1016/J.SOLENER.2017.02.056.

[23] Solar Energy Fundamentals and Design: with Computer Applications - AbeBooks - Stine, William B.; Harrigan, Raymond W.: 0471887188 n.d.

[24] B. Kongtragool, S. Wongwises, Optimum absorber temperature of a once-reflecting full conical concentrator of a low temperature differential Stirling engine, Renew. Energy 30 (2005) 1671–1687, https://doi.org/10.1016/j.renene.2005.01.003.

[25] U.R. Singh, A. Kumar, Review on solar Stirling engine: development and performance, Therm. Sci. Eng. Prog. 8 (2018) 244–256, https://doi.org/10.1016/J.TSEP.2018.08.016.

[26] M.H. Ahmadi, A.H. Mohammadi, S. Dehghani, M.A. Barranco-Jimenez, Multi-objective thermodynamic-based optimization of output power of Solar Dish-Stirling engine by implementing an evolutionary algorithm, Energy Convers. Manag. 75 (2013) 438–445, https://doi.org/10.1016/j.enconman.2013.06.030.

[27] L.S. Mendoza Castellanos, G.E. Carrillo Caballero, V.R. Melian Cobas, E.E. Silva Lora, A.M. Martinez Reyes, Mathematical modeling of the geometrical sizing and thermal performance of a Dish/Stirling system for power generation, Renew. Energy 107 (2017) 23–35, https://doi.org/10.1016/j.renene.2017.01.020.

[28] A.Z. Hafez, A. Soliman, K.A. El-Metwally, I.M. Ismail, Solar parabolic dish Stirling engine system design, simulation, and thermal analysis, Energy Convers. Manag. 126 (2016) 60–75, https://doi.org/10.1016/j.enconman.2016.07.067.

[29] G.E. Carrillo Caballero, L.S. Mendoza, A.M. Martinez, E.E. Silva, V.R. Melian, O. J. Venturini, et al., Optimization of a Dish Stirling system working with DIR-type receiver using multi-objective techniques, Appl. Energy 204 (2017) 271–286, https://doi.org/10.1016/j.apenergy.2017.07.053.

[30] M.Z. Malik, P.H. Shaikh, S. Zhang, A.A. Lashari, Z.H. Leghari, M.H. Baloch, et al., A review on design parameters and specifications of parabolic solar dish Stirling systems and their applications, Energy Rep. 8 (2022) 4128–4154, https://doi.org/10.1016/j.egyr.2022.03.031.

[31] Y. Bravo, C. Monné, N. Bernal, M. Carvalho, F. Moreno, M. Muñoz, Hybridization of solar dish-stirling technology: analysis and design, Environ Prog \& Sustain Energy 33 (2014) 1459–1466.

[32] C. Monné, Y. Bravo, F. Moreno, M. Munoz, Analysis of a solar dish–Stirling system with hybridization and thermal storage, Int J Energy Environ Eng 5 (2014) 1–5.

[33] J. Hartenstine, P. Dussinger, Development of a solar and gas-fired heat pipe receiver for the Cummins power generation 7.5 kWe dish/Stirling system, Intersoc. Energy Convers. Eng. Conf. (1994) 3864.

[34] R. Blazquez, J. Carballo, M. Silva, Optical design and optimization of parabolic dish solar concentrator with a cavity hybrid receiver, AIP Conf Proc 1734 (2016), https://doi.org/10.1063/1.4949149.

[35] Barbosa D, André P, Antunes P, Paixão T, Marques C, van Ardenne A, et al. BIOSTIRLING-4SKA: A Cost Effective and Efficient Approach for a New Generation of Solar Dish-Stirling Plants Based on Storage and Hybridization; an Energy Demo Project for Large Scale Infrastructures. ArXiv Prepr ArXiv171203029 2017.

[36] M. Kang, J. Kim, Y. Kang, N. Kim, S. Yoo, J. Kim, An experimental study on the heat transfer characteristics of the hybrid solar receiver for a dish concentrating system, Proc. ISES World Congr V (2008) 689–693, 2007 (Vol. I–.
[37] D. Laing, M. Pålsson, Hybrid dish/Stirling systems: combustor and heat pipe receiver development, J Sol Energy Eng 124 (2002) 176–181.
[38] J. Moreno, S. Rawlinson, C. Andraka, M. Mehos, M.S. Bohn, J. Corey, Dish/Stirling Hybrid-Receiver Sub-scale Tests and Full-Scale Design, 1999.
[39] Y. Kadri, H. Hadj Abdallah, Performance evaluation of a stand-alone solar dish Stirling system for power generation suitable for off-grid rural electrification, Energy Convers Manag 129 (2016) 140–156, https://doi.org/10.1016/j.enconman.2016.10.024.
[40] A.B. Swedish Stirling, n.d, https://swedishstirling.com/en/. (Accessed 7 May 2023).
[41] C.S. Blázquez, D. Borge-Diez, I.M. Nieto, A.F. Martín, D. González-Aguilera, Multi-parametric evaluation of electrical, biogas and natural gas geothermal source heat pumps, Renew Energy 163 (2021) 1682–1691, https://doi.org/10.1016/j.renene.2020.10.080.
[42] Environment - U.S. Energy Information Administration (EIA) - U.S. Energy Information Administration (EIA) n.D.
[43] A. Giuliano, C. Freda, E. Catizzone, Techno-economic assessment of bio-syngas production for methanol synthesis: a focus on the water–gas shift and carbon capture sections, Bioengineering 7 (2020) 1–18, https://doi.org/10.3390/bioengineering7030070.
[44] N. Couto, A. Rouboa, V. Silva, E. Monteiro, K. Bouziane, Influence of the biomass gasification processes on the final composition of syngas, Energy Procedia 36 (2013) 596–606, https://doi.org/10.1016/j.egypro.2013.07.068.
[45] Meteonorm Meteonorm, Global Meteorological Database. Handboo Part II: Theory, 2015. Version 7.1.7.21517.
[46] K. Lovegrove, J. Pye, Fundamental Principles of Concentrating Solar Power (CSP) Systems, 2012, pp. 16–67. Conc. Sol. power Technol., Elsevier.
[47] J.M. Honig, Chapter 1 - fundamentals, in: J.M. Honig (Ed.), Thermodyn, third ed. third ed., Academic Press, Amsterdam, 2007, pp. 1–110, https://doi.org/10.1016/B978-012373877-6/50003-4.
[48] L. Qiu, M. Yan, Research on Primary Energy Ratio of the Gas Engine-Driven Heat Pump under Different Run Mode, 2010, pp. 1–4, https://doi.org/10.1109/APPEEC.2010.5449018, 2010 Asia-Pacific Power Energy Eng. Conf.
[49] Elettrocostruzioni s.r.l, n.d, https://www.elettrocostruzionisrl.it/.
[50] Horizon s.r.l, n.d, https://horizonfirm.com/it/home-ita/.
[51] M.K. Selcuk, T. Fujita, A Nomographic Methodology for Use in Performance Trade-Off Studies of Parabolic Dish Solar Power Modules, 1984.
[52] C.W. Lopez, K.W. Stone, Performance of the Southern California Edison Company Stirling Dish, vol. 94, NASA STI/Recon Tech Rep N, 1993.
[53] A. Buscemi, V. Lo Brano, C. Chiaruzzi, G. Ciulla, C. Kalogeri, A validated energy model of a solar dish-Stirling system considering the cleanliness of mirrors, Appl Energy (2020), https://doi.org/10.1016/j.apenergy.2019.114378.
[54] S.A. Klein, TRNSYS 17: A Transient System Simulation Program, vol. 1, Sol Energy Lab Univ Wisconsin, Madison, USA, 2010.
[55] Lanchi M., Falchetta M., Montecchi M., Russo V., Crescenzi T. MA. D2.2 Technical Report on Steady State Simulation, OMSoP project. (n.d).
[56] D.W. Green, M.Z. Southard, Perry's Chemical Engineers' Handbook, McGraw-Hill Education, 2019.
[57] M. Khader, D1.8 – Optimised Radial Turbine Design, 2014.
[58] M. Lanchi, J. Al-Zaili, V. Russo, M. Falchetta, M. Montecchi, L. Aichmayer, A quasi-steady state model of a solar parabolic dish micro gas turbine demonstration plant, Energies 15 (2022), https://doi.org/10.3390/en15031059.